J|A|C|S
ARTICLES
Published on Web 12/05/2001

C−H Bond Activation by a Ferric Methoxide Complex: Modeling the Rate-Determining Step in the Mechanism of Lipoxygenase

Christian R. Goldsmith, Robert T. Jonas, and T. Daniel P. Stack*

Contribution from the Department of Chemistry, Stanford University, Stanford, California 94305

Received June 19, 2001

Abstract: Lipoxygenases are mononuclear non-heme iron enzymes that regio- and stereospecifcally convert 1,4-pentadiene subunit-containing fatty acids into alkyl peroxides. The rate-determining step is generally accepted to be hydrogen atom abstraction from the pentadiene subunit of the substrate by an active ferric hydroxide species to give a ferrous water species and an organic radical. Reported here are the synthesis and characterization of a ferric model complex, [Fe^{III}(**PY5**)(OMe)](OTf)$_2$, that reacts with organic substrates in a manner similar to the proposed enzymatic mechanism. The ligand **PY5** (2,6-bis(bis(2-pyridyl)methoxymethane)pyridine) was developed to simulate the histidine-dominated coordination sphere of mammalian lipoxygenases. The overall monoanionic coordination provided by the endogenous ligands of lipoxygenase confers a strong Lewis acidic character to the active ferric site with an accordingly positive reduction potential. Incorporation of ferrous iron into **PY5** and subsequent oxidation yields a stable ferric methoxide species that structurally and chemically resembles the proposed enzymatic ferric hydroxide species. Reactivity with a number of hydrocarbons possessing weak C−H bonds, including a derivative of the enzymatic substrate linoleic acid, scales best with the substrates' bond dissociation energies, rather than pK_a's, suggesting a hydrogen atom abstraction mechanism. Thermodynamic analysis of [Fe^{III}(**PY5**)(OMe)](OTf)$_2$ and the ferrous end-product [Fe^{II}(**PY5**)(MeOH)](OTf)$_2$ estimates the strength of the O−H bond in the metal bound methanol in the latter to be 83.5 ± 2.0 kcal mol^{-1}. The attenuation of this bond relative to free methanol is largely due to the high reduction potential of the ferric site, suggesting that the analogously high reduction potential of the ferric site in LO is what allows the enzyme to perform its unique oxidation chemistry. Comparison of [Fe^{III}(**PY5**)(OMe)](OTf)$_2$ to other coordination complexes capable of hydrogen atom abstraction shows that, although a strong correlation exists between the thermodynamic driving force of reaction and the rate of reaction, other factors appear to further modulate the reactivity.

Introduction

Lipoxygenases (LOs) are mononuclear non-heme iron enzymes, found in both plants and animals, that catalyze the regio- and stereospecific dioxygenation of *cis*,*cis*-1,4-pentadiene-containing fatty acids to alkyl hydroperoxides. Linoleic acid, the natural substrate for most plant LOs, is oxygenated with positional stereospecificity to produce hydroperoxyoctadecadienoic acids, completing the first step in the biosynthesis of the growth-regulation substance jasmonic acid and of the wound-healing compounds traumatin and traumatic acid (Scheme 1).[1] Mammalian LOs initiate the synthesis of physiological effectors, such as leukotrienes and lipoxins, from arachidonic acid. The inhibition of human LO activity is of considerable interest to pharmaceutical concerns, as various LOs have been implicated in inflammatory conditions, such as arthritis, bronchial asthma, and atherosclerosis.[1] Recently, LO inhibitors have also been found to inhibit tumor growth.[2,3]

Scheme 1

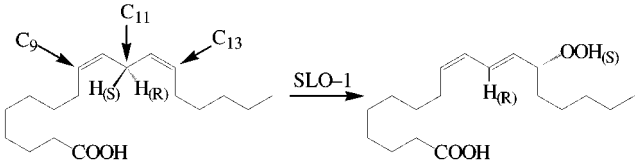

Linoleic Acid 13–HPOD

The iron-binding ligands of the LOs have been determined by sequence homology and crystallographic determinations. X-ray structures of two plant isozymes, soybean lipoxygenase-1 (SLO-1) and soybean lipoxygenase-3 (SLO-3), are known.[4−6] Three imidazole nitrogens of histidine residues, an amide oxygen of an asparagine residue, and the carboxylate oxygen of the C-terminus residue constitute the endogenous, peptide-based ligands of the metal center. Protein sequence comparisons of

* To whom correspondence should be addressed. Tel.: (650) 725-8736. Fax: (650) 725-0259. E-mail: stack@stanford.edu.

(1) Nelson, M. J.; Seitz, S. P. In *Active Oxygen in Biochemistry*; Valentine, J. S., Foote, C. S., Greenberg, A., Liebman, J. F., Eds.; Blackie Academic & Professional: London, 1995; Vol. 3.
(2) Castonguay, A.; Rioux, N. *Carcinogenesis* **1998**, *19*, 1393−1400.
(3) Adrian, T. E.; Ding, X. Z.; Iverson, P.; Cluck, M. W.; Knezetic, J. A. *Biochem. Biophys. Res. Commun.* **1999**, *261*, 218−223.
(4) Skrzypczak-Jankun, E.; Amzel, L. M.; Kroa, B. A.; Funk, M. O., Jr. *Proteins: Struct., Funct. Genet.* **1997**, *29*, 15−31.
(5) Minor, W.; Steczko, J.; Stec, B.; Otwinowski, Z.; Bolin, J. T.; Walter, R.; Axelrod, B. *Biochemistry* **1996**, *35*, 10687−10701.

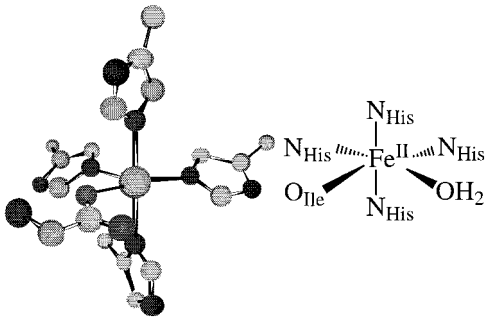

Figure 1. Three-dimensional representation of the non-heme iron site of rabbit 15-lipoxygenase as determined by crystallography, including a scheme of the ligand coordination set. Fe−N(His) distances average 2.2 Å. The Fe−O(Ile) distance is 2.1 Å.[9]

over 20 LOs from both plants and animals reveal the near conservation of the five structurally characterized iron-binding ligands. An exception is found for the 15-lipoxygenases from humans and rabbits, in which the asparagine amide oxygen is replaced by the imidazole nitrogen of a histidine residue.[7,8] The reported X-ray structure of rabbit 15-lipoxygenase (15-LO) confirms that the endogenous ligation consists of four imidazole nitrogens and a carboxylate oxygen (Figure 1).[9]

Spectroscopic studies have investigated the iron coordination differences between the resting and active forms of the LO enzymes. The isolated resting forms of soybean and mammalian LOs contain a high-spin Fe(II) center.[10−12] Spectroscopic data of SLO-1 indicate that the iron center exists as a mixture of five- and six-coordinate species in solution with possible detachment of the asparagine-derived ligand from the iron center.[1] Though not observed in the crystal structures, an exogenous water molecule likely completes the octahedral coordination of the Fe(II) center.[5] Unlike many of the mononuclear non-heme iron enzymes, the ferrous form, Fe(II), of LO is inactive, and the iron center must be oxidized to the ferric state, Fe(III), for catalytic activity.[1] Autoactivation of SLO occurs in the presence of the hydroperoxy product of linoleic acid.[1] Extended X-ray absorption fine structure (EXAFS) and magnetic circular dichroism studies on the Fe(III) form of SLO-1 indicate a six-coordinate metal center.[1] EXAFS studies reveal the presence of a short iron−ligand bond distance of 1.88 Å that is attributed to a single hydroxide ligand.[13] The histidine-for-asparagine substitution from plant to mammalian LO results in a more stabilized six-coordinate Fe(III) species, the increased stability being attributed to the stronger electron donation of an imidazole ligand relative to an amide oxygen.[14,15] The stabilized Fe(III) center may explain the reduced reactivity of the mammalian LOs relative to plant LOs. Selective mutation of the coordinating asparagine to histidine in SLO-1 supports this hypothesis. The N694H SLO-1 mutant has a $k_{cat} \approx 10 \pm 2$ s^{-1}, more similar to the rate of 15-human LO ($k_{cat} \approx 6.2 \pm 0.1$ s^{-1}) than the wild-type SLO-1 ($k_{cat} \approx 280 \pm 8$ s^{-1}).[16]

LO is one of a limited number of mononuclear non-heme iron enzymes in which catalysis is proposed to occur through substrate activation rather than O_2 activation.[17] A kinetic isotope effect (KIE) of greater than 50 is measured for the LO catalytic cycle (305 K), indicating that C−H bond cleavage is involved in the rate-determining step (RDS).[18−21] In the enzyme, two additional processes are found to be partially rate determining at 298 K in the catalytic cycle: substrate binding and dissociation, and a yet to be identified solvent-sensitive step.[22] As the solvent temperature is increased, the viscosity of the system decreases until, at 310 K, the C−H bond cleavage reaction is fully rate limiting. In the generally accepted mechanism, the RDS involves hydrogen atom abstraction (HA) from the fatty acid substrate with concomitant reduction of the ferric−hydroxide center to a ferrous−water species and formation of a fatty acid radical (Scheme 2).[1] Another mechanism, involving an organometallic ferric species, has also been proposed.[23] Diffusion-limited trapping of the radical intermediate by O_2 followed by oxidation of the ferrous−water species to the ferric−hydroxide species by the peroxyl radical completes the catalytic cycle.

While stereospecific C−H bond activation of the *cis*,*cis*-1,4-pentadiene subunit has been established during LO activity, the characterization of the resulting substrate radical is limited.[1] Kinetic experiments indicate that C−H bond cleavage occurs prior to the incorporation of O_2 by the activated substrate−enzyme complex.[24,25] Starting with the fatty acid substrate linoleic acid, the stereospecific product 13(*S*)-hydroperoxy-9(*Z*),11(*E*)-octadecadienoic acid (13-HPOD) results from SLO-1 activity (Scheme 1); in contrast, autoxidation of linoleic acid radicals in the absence of enzyme results in multiple regio- and stereoisomer hydroperoxide products.[26,27]

While the reaction of free radicals with O_2 is well known, few metal-based systems are known to perform C−H bond activation through a well-characterized HA mechanism. Such a mechanism has been identified for the reactions of chromyl chloride and permanganate metal−oxo species with simple organic substrates.[28−32] More recently, a ferric tris(2,2′-bi-

(6) Boyington, J. C.; Gaffney, B. J.; Amzel, L. M. *Science* **1993**, *260*, 1482−1486.
(7) Fleming, J.; Thiele, B. J.; Chester, J.; O'Prey, J.; Janetzki, S.; Aitken, A.; Anton, I. A.; Rapoport, S. M.; Harrison, P. R. *Gene* **1989**, *79*, 181−188.
(8) Sigal, E.; Craik, C. S.; Highland, E.; Grunberger, D.; Costello, L. L.; Dixon, R. A. F.; Nadel, J. A. *Biochem. Biophys. Res. Commun.* **1988**, *157*, 457−464.
(9) Gillmor, S. A.; Villaseñor, A.; Fletterick, R.; Sigal, E.; Browner, M. F. *Nat. Struct. Biol.* **1997**, *4*, 1003−1009.
(10) Slappendel, S.; Malmström, B. G.; Petersson, L.; Ehrenberg, A.; Veldink, G. A.; Vliegenthart, J. F. G. *Biochem. Biophys. Res. Commun.* **1982**, *108*, 673−677.
(11) Axelrod, B.; Cheesbrough, T. M.; Laaskso, S. *Methods Enzymol.* **1981**, *71*, 441−451.
(12) Pistorius, E. K.; Axelrod, B. *J. Biol. Chem.* **1974**, *249*, 3183−3186.
(13) Scarrow, R. C.; Trimitsis, M. G.; Buck, C. P.; Grove, G. N.; Cowling, R. A.; Nelson, M. J. *Biochemistry* **1994**, *33*, 15023−15035.
(14) Zhang, Y.; Gan, Q.-F.; Pavel, E. G.; Sigal, E.; Solomon, E. I. *J. Am. Chem. Soc.* **1995**, *117*, 7422−7427.
(15) Pavlosky, M. A.; Zhang, Y.; Westre, T. E.; Gan, Q.-F.; Pavel, E. G.; Campochiaro, C.; Hedman, B.; Hodgson, K. O.; Solomon, E. I. *J. Am. Chem. Soc.* **1995**, *117*, 4316−4327.
(16) Holman, T. R.; Zhou, J.; Solomon, E. I. *J. Am. Chem. Soc.* **1998**, *120*, 12564−12572.
(17) Que, L., Jr.; Ho, R. Y. N. *Chem. Rev.* **1996**, *96*, 2607−2624.
(18) Jonsson, T.; Glickman, M. H.; Sun, S. J.; Klinman, J. P. *J. Am. Chem. Soc.* **1996**, *118*, 10319−10320.
(19) Glickman, M. H.; Wiseman, J. S.; Klinman, J. P. *J. Am. Chem. Soc.* **1994**, *116*, 793−794.
(20) Hwang, C.-C.; Grissom, C. B. *J. Am. Chem. Soc.* **1994**, *116*, 795−796.
(21) Lewis, E. R.; Johansen, E.; Holman, T. R. *J. Am. Chem. Soc.* **1999**, *121*, 1395−1396.
(22) Glickman, M. H.; Klinman, J. P. *Biochemistry* **1995**, *34*, 14077−14092.
(23) Corey, E. J.; Nagata, R. *J. Am. Chem. Soc.* **1987**, *109*, 8107−8108.
(24) Glickman, M. H.; Cliff, S.; Thiemens, M.; Klinman, J. P. *J. Am. Chem. Soc.* **1997**, *119*, 11357−11361.
(25) Glickman, M. H.; Klinman, J. P. *Biochemistry* **1996**, *35*, 12882−12892.
(26) Porter, N. A. *Acc. Chem. Res.* **1986**, *19*, 262−268.
(27) Porter, N. A.; Wujek, D. G. *J. Am. Chem. Soc.* **1984**, *106*, 2626−2629.
(28) Gardner, K. A.; Kuehnert, L. L.; Mayer, J. M. *Inorg. Chem.* **1997**, *36*, 2069−2078.
(29) Cook, G. K.; Mayer, J. M. *J. Am. Chem. Soc.* **1995**, *117*, 7139−7156.
(30) Gardner, K. A.; Mayer, J. M. *Science* **1995**, *269*, 1849−1851.

Scheme 2

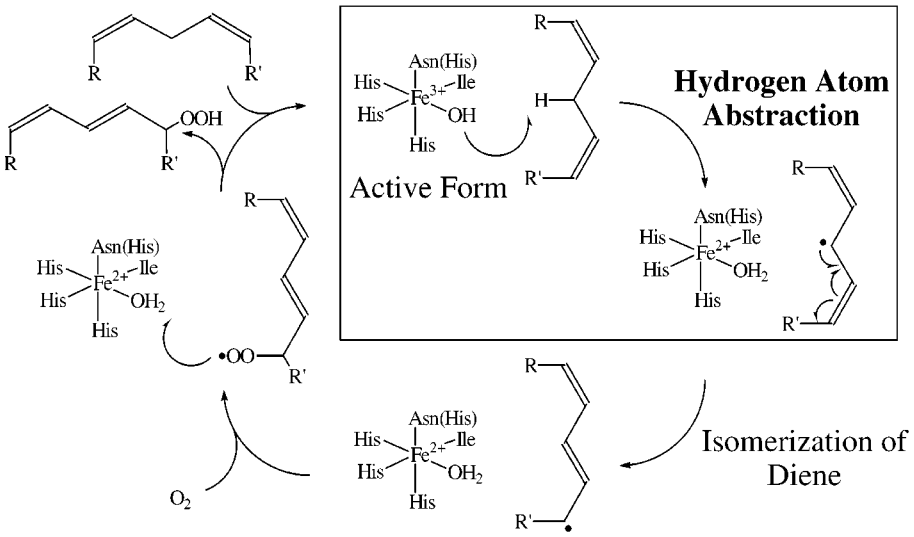

imidazoline) system has been shown to exhibit similar reactivity.[33] In these studies, a thermodynamic bond strength approach, similar to that used to determine the homolytic X−H bond dissociation energy in many organic and organometallic[34] compounds, provides an understanding of the HA ability of a metal complex. Three primary factors affect the driving force for metal-based HA: the redox potential of the metal center, the strength of the substrate C−H bond broken, and the energy of the O−H (or N−H) bond formed in the reduced metal complex.

This study focuses on a pentadentate ligand designed and synthesized to mimic specific attributes of the iron coordination site in the LOs, namely a five-coordinate, square pyramidal, endogenous environment that can accommodate a sixth exogenous ligand. Using a pentapyridyl ligand, 2,6-bis(bis(2-pyridyl)-methoxymethane)pyridine (**PY5**), an Fe(III) complex with an axial methoxide ligand, $[Fe^{III}(\mathbf{PY5})(OMe)](OTf)_2$ (**2**) (OTf = triflate, $CF_3SO_3^-$), has been synthesized. This model complex shares many similar structural and spectroscopic properties with the LOs. Additionally, **2** promotes the cleavage of weak C−H bonds of substrates with concomitant reduction of the iron center to the ferrous complex $[Fe^{II}(\mathbf{PY5})(MeOH)](OTf)_2$ (**1**). The reactivity profile is consistent with a HA mechanism, providing chemical precedent for the C−H bond activation step in the proposed mechanism of LO.[35] The chemical similarities of this model complex to the iron site in LOs strongly support the HA mechanism by a ferric−hydroxide species in the native system.

Results and Analysis

Ferric Complex Synthesis. In an effort to isolate structurally and functionally relevant analogues of LO enzymes, the pentadentate ligand, 2,6-bis(bis(2-pyridyl)methoxymethane)-pyridine (**PY5**), was designed and synthesized.[35,36] The ligand is composed of five pyridine subunits and accommodates a single metal ion in a nearly idealized square pyramidal coordination geometry. $[Fe^{II}(\mathbf{PY5})(MeOH)](OTf)_2$ (**1**) is isolated directly from an equimolar mixture of $Fe^{II}(OTf)_2$ and **PY5** in methanol (MeOH). Addition of either H_2O_2 or iodosobenzene to a yellow solution of **1** in MeOH results in the formation of the orange ferric complex $[Fe^{III}(\mathbf{PY5})(OMe)](OTf)_2$ (**2**). A UV/

$$[Fe^{II}(\mathbf{PY5})(MeOH)]^{2+} \xrightarrow{0.5H_2O_2 \text{ or } C_6H_5IO} [Fe^{III}(\mathbf{PY5})(OMe)]^{2+} \quad (1)$$

vis spectroscopic titration of the oxidation of **1** indicates that the reaction is complete after addition of 0.5 equiv of H_2O_2 or iodosobenzene. Addition of >1.5 equiv of H_2O_2 to **1** gives a thermally unstable blue species that is proposed to be a low-spin hydroperoxide-bound ferric species, $[Fe^{III}(\mathbf{PY5})(OOH)](OTf)_2$.[36,37] The methoxy complex, **2**, is isolated as a stable red/

$$[Fe^{II}(\mathbf{PY5})(MeOH)]^{2+} \xrightarrow{\text{excess } H_2O_2} [Fe^{III}(\mathbf{PY5})(OOH)]^{2+} \quad (2)$$

orange powder in high yield (75%). The aerobic and thermal stability of **2** is unusual, as no other ferric complex with **PY5** has been successfully isolated to date.

Solid State Structure. Structural and refinement data for the crystal structures of the free ligand **PY5**, **1**, and **2** are summarized in Table 1. The atom labeling scheme of the ligand in all three structures is congruent in order to facilitate comparison of the structural parameters. Both iron centers of **1** and **2** are coordinated in an octahedral environment, with the five nitrogen donors of **PY5** in a square pyramidal arrangement and an oxygen atom of a methanol (**1**) or a methoxide (**2**) completing the coordination sphere. For the purpose of discussion, an equatorial plane ($\mathbf{Pl_{eq}}$) is defined by the least-squares plane of the four nitrogen atoms $\mathbf{N_{2\rightarrow5}}$ in their respective pyridine subunits $\mathbf{Py_{2\rightarrow5}}$, such that the axial positions are occupied by $\mathbf{N_1}$ of $\mathbf{Py_1}$ and the heteroatom of the exogenous ligand.

$[Fe^{II}(\mathbf{PY5})(MeOH)](OTf)_2 \cdot (MeOH)$ was crystallized as a stable yellow/green prismatic solid with an asymmetric unit containing the cation $[Fe^{II}(\mathbf{PY5})(MeOH)]^{2+}$, two triflate anions, and a MeOH solvate molecule. The hydrogen atom of the coordinated MeOH was located by a difference Fourier map and is involved in a hydrogen-bonding network with the MeOH of solvation, which in turn hydrogen bonds to one of the triflate

(31) Cook, G. K.; Mayer, J. M. *J. Am. Chem. Soc.* **1994**, *116*, 1855−1868.
(32) Mayer, J. M. *Acc. Chem. Res.* **1998**, *31*, 441−450.
(33) Roth, J. P.; Mayer, J. M. *Inorg. Chem.* **1999**, *38*, 2760−2761.
(34) Astruc, D.; Trujillo, H. A.; Casado, C. M.; Ruiz, J. *J. Am. Chem. Soc.* **1999**, *121*, 5674−5686.
(35) Jonas, R. T.; Stack, T. D. P. *J. Am. Chem. Soc.* **1997**, *119*, 8566−8567.
(36) deVries, M. E.; LaCrois, R. M.; Roelfes, G.; Kooijman, H.; Spek, A. L.; Hage, R.; Feringa, B. L. *Chem. Commun.* **1997**, 1549−1550.
(37) Unpublished results.

Table 1. Crystallographic Data for **PY5**, [Fe^{II}(**PY5**)(MeOH)](OTf)$_2$, and [Fe^{III}(**PY5**)(OMe)](OTf)$_2$

complex	**PY5**	[Fe(**PY5**)(MeOH)] (OTf)$_2$·(MeOH)	[Fe(**PY5**)(OMe)] (OTf)$_2$·(MeOH)
formula	$C_{29}H_{25}N_5O_2$	$C_{33}H_{33}N_5O_{10}F_6S_2Fe$	$C_{33}H_{32}N_5O_{10}F_6S_2Fe$
FW (g mol^{-1})	475.55	893.61	892.60
crystal system	monoclinic	triclinic	triclinic
space group	*Cc* (No. 9)	$P\bar{1}$ (No. 2)	$P\bar{1}$ (No. 2)
a (Å)	11.017(1)	12.417(2)	9.532(2)
b (Å)	13.626(1)	12.672(2)	9.966(1)
c (Å)	16.527(1)	13.345(1)	19.852(3)
α (deg)	90.00	80.00(1)	96.17(1)
β (deg)	107.50(3)	63.509(9)	100.12(2)
γ (deg)	90.00	89.51(1)	92.53(2)
volume (Å^3)	2366.2(5)	1845.1(5)	1841.8(5)
Z	4	2	2
μ_{calc} (cm^{-1})	0.87	6.16	6.20
ρ_{obs} (ρ_{calc}) (g cm^{-3})	1.320 (1.335)	>1.590 (1.608)	>1.590 (1.609)
crystal size (mm)	0.50 × 0.60 × 0.50	0.50 × 0.50 × 0.70	0.20 × 0.50 × 0.70
2θ range	10.0° < 2θ < 50.0°	10.0° < 2θ < 50.0°	10.0° < 2θ < 50.0°
reflections collected	2295	6790	7985
unique reflections	2184 (R_{int} = 0.0343)	6472 (R_{int} = 0.0579)	6454 (R_{int} = 0.0385)
reflections with ($F_o^2 > 3.00\sigma(F_o^2)$)	1379	5613	4593
number of parameters	321	514	597
reflns/params ratio	4.30	10.92	7.69
R^a	0.041	0.053	0.059
$R_w{}^a$	0.028	0.074	0.062

[a] $R = \sum||F_o| - |F_c||/\sum|F_o|$; $R_w = [\sum w(|F_o| - |F_c|)^2/\sum wF_o^2)^{1/2}$, where $w = 4F_o^2/\sigma^2(F_o^2)$; $\sigma^2(F_o^2) = S^2(C + R^2B) + (pF_o^2)^2/(Lp)^2$, with S = scan rate, C = total integrated peak count, R = ratio of scan time to background counting time, B = total background count, Lp = Lorentz polarization factor, and p = p factor (0.002 for **PY5**, 0.008 for [Fe^{II}(**PY5**)(MeOH)](OTf)$_2$, and 0.006 for [Fe^{III}(**PY5**)(OMe)](OTf)$_2$).

Table 2. Selected Bond Distances and Bond Angles for [Fe^{II}(**PY5**)(MeOH)](OTf)$_2$ (**1**) and [Fe^{III}(**PY5**)(OMe)](OTf)$_2$ (**2**)

bond lengths (Å)			bond angles (deg)		
	1	**2**		**1**	**2**
Fe1−N1	2.097(3)	2.147(4)	N1−Fe1−N2	85.0(1)	81.2(1)
Fe1−N2	2.152(3)	2.154(4)	N1−Fe1−N3	86.2(1)	85.5(1)
Fe1−N3	2.203(3)	2.178(4)	N2−Fe1−N3	83.2(1)	82.8(1)
Fe1−N4	2.217(3)	2.223(4)	N4−Fe1−N5	82.1(1)	81.4(1)
Fe1−N5	2.141(4)	2.107(4)	N2−Fe1−N5	97.7(1)	95.8(2)
Fe1−O3	2.040(3)	1.782(3)	N3−Fe1−N4	95.7(1)	97.8(1)
O3−C30	1.422(6)	1.375(7)	N2−Fe1−N4	170.5(1)	163.9(1)
			N3−Fe1−N5	171.9(1)	172.1(2)
			N2−Fe1−O3	93.6(1)	98.8(2)
			N3−Fe1−O3	90.2(1)	92.4(2)
			N1−Fe1−O3	176.3(1)	177.9(2)
			Fe1−O3−C30	134.0(3)	164.9(4)

[a] Estimated standard deviations in the least-squares figure are given in parentheses.

anions. The anion count and the identity of the exogenous ligand as MeOH rather than methoxide are consistent with a ferrous complex. The average value for the five Fe(1)−N(1 → 5) bond lengths (2.162(3) Å) is also consistent with the assignment of a high-spin (*hs*) Fe(II) center in this complex.[38,39] Figure 2B shows an ORTEP representation of [Fe^{II}(**PY5**)(MeOH)]$^{2+}$ with selected bond lengths and angles provided in Table 2. The Fe(1)−O(3) bond length of 2.040(3) Å and the Fe(1)−O(3)−C(30) bond angle of 134° for the exogenous MeOH ligand lie at the extremes for characterized divalent transition metals.[40−43] The selected view of **1** highlights the deviation of the metal-bound **PY5** ligand from the idealized C_{2v} symmetry of the free ligand structure (Figure 2A).

In the structure of free ligand, the plane of **Py$_1$** and the methoxy groups are effectively coplanar. The two methoxy-methyl groups adopt a trans conformation, yielding an overall pseudo-C_2-symmetric conformation. Positioning of the methoxy-methyl groups in the clefts created between **Py$_2$** and **Py$_3$** and between **Py$_4$** and **Py$_5$** results in predictable structural deviations at the quaternary carbon centers (C_{quat}); the C(**Py$_2$**)−C_{quat}−C(**Py$_3$**) and C(**Py$_4$**)−C_{quat}−C(**Py$_5$**) angles are greater than the anticipated idealized tetrahedral angle. This "noninnocent" positioning of the methoxy-methyl groups in other related ligands has been previously noted,[44] and these structural deviations are accentuated upon metal chelation (vide infra).

The most curious aspects of the [Fe^{II}(**PY5**)(MeOH)]$^{2+}$ structure are the tilting of the **Py$_1$** plane relative to the **Pl$_{eq}$** plane (19.4° from the perpendicular of **Pl$_{eq}$**) and the opposing position of both methoxy-methyl groups to this tilt (Figure 2B). These structural distortions result from the position of the two methoxy-methyl groups in the clefts between **Py$_2$** and **Py$_1$** and between **Py$_5$** and **Py$_1$**. The C(**Py$_2$**)−C_{quat}−C(**Py$_1$**) and C(**Py$_5$**)−C_{quat}−C(**Py$_1$**) angles distort from ∼108° in free **PY5** to ∼118° in **1** in order to accommodate the methoxy groups. This tilting is also associated with consistent metrical distortions in the Fe−**N$_{eq}$** bond distances; the Fe−**N$_{eq}$** bonds opposite to the **Py$_1$** tilt (Fe−**N$_2$**, 2.152(3) Å; Fe−**N$_5$**, 2.141(4) Å) are significantly shorter than the other two Fe−**N$_{eq}$** distances (Fe−**N$_3$**, 2.203(3) Å; Fe−**N$_4$**, 2.217(3) Å). The noninnocent positioning of the methoxy-methyl groups provides a mechanism of mechanical coupling within **PY5** such that each half of the ligand works in concert to ligate a metal.

[Fe^{III}(**PY5**)(OMe)](OTf)$_2$·(MeOH) was crystallized as a stable red/orange prismatic solid. The asymmetric unit contains a dication [Fe^{III}(**PY5**)(OMe)]$^{2+}$, two triflate anions, and a MeOH

(38) Que, L., Jr.; Zang, Y.; Kim, J.; Dong, Y.; Wilkinson, E. C.; Appelman, E. H. *J. Am. Chem. Soc.* **1997**, *119*, 4197−4205.
(39) Que, L., Jr.; Roelfes, G.; Lubben, M.; Chen, K.; Ho, R. Y. N.; Meetsma, A.; Genseberger, S.; Hermant, R. M.; Hage, R.; Mandal, S. K.; Young, V. G., Jr.; Zang, Y.; Kooijman, H.; Spek, A. L.; Feringa, B. L. *Inorg. Chem.* **1999**, *38*, 1929−1936.
(40) Bruce, M. I.; Walton, J. K.; Williams, M. L.; Patrick, J. M.; Skelton, B. W.; White, A. H. *J. Chem. Soc., Dalton Trans.* **1983**, 815−821.
(41) Cotton, F. A.; Duraj, S. A.; Manzer, L. E.; Roth, W. J. *J. Am. Chem. Soc.* **1985**, *107*, 3850−3855.
(42) Noro, S.; Kondo, M.; Ishii, T.; Kitagawa, S.; Matsuzaka, H. *J. Chem. Soc., Dalton Trans.* **1999**, 1569−1574.
(43) Mandal, S. K.; Que, L., Jr. *Inorg. Chem.* **1997**, *36*, 5424−5425.
(44) Jonas, R. T.; Stack, T. D. P. *Inorg. Chem.* **1998**, *37*, 6615−6629.

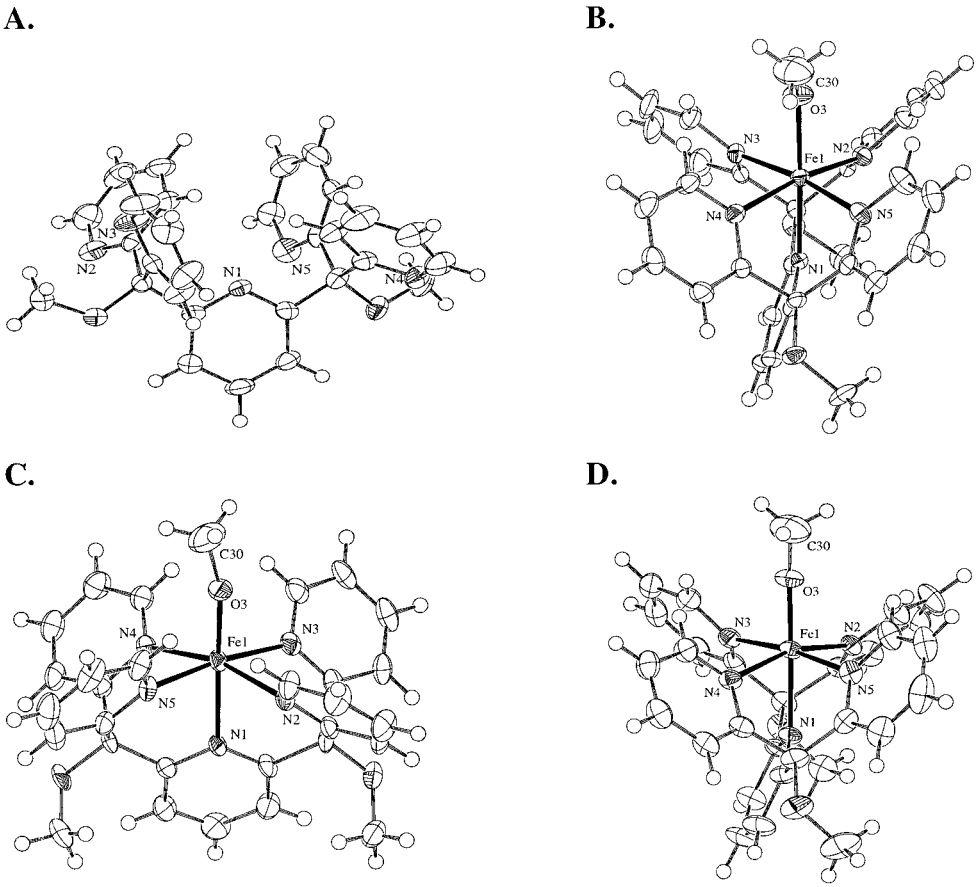

Figure 2. Representations of the crystal structures of (A) the free ligand **PY5**, (B) the dication $[Fe^{II}(\mathbf{PY5})(MeOH)]^{2+}$, and (C,D) two 90° views of the dication $[Fe^{III}(\mathbf{PY5})(OMe)]^{2+}$. Ellipsoids drawn at the 50% probability level.

solvate molecule. As with **1**, a strong hydrogen-bonding network is developed among the anions and the MeOH of solvation. Two orthogonal views of $[Fe^{III}(\mathbf{PY5})(OMe)]^{2+}$ are shown in Figure 2C,D, and selected bond lengths and angles are provided in Table 2. Similar to the structure of $[Fe^{II}(\mathbf{PY5})(MeOH)]^{2+}$, the plane of $\mathbf{Py_1}$ in $[Fe^{III}(\mathbf{PY5})(OMe)]^{2+}$ tilts relative to the perpendicular of $\mathbf{Pl_{eq}}$ by 20.2°, and the two methoxy-methyl groups are positioned between $\mathbf{Py_2}$ and $\mathbf{Py_1}$ and between $\mathbf{Py_5}$ and $\mathbf{Py_1}$. The C($\mathbf{Py_2}$)−C_{quat}−C($\mathbf{Py_1}$) and C($\mathbf{Py_5}$)−C_{quat}−C($\mathbf{Py_1}$) angles distort from ∼108° in the free ligand to ∼117° in **2**, and the contraction of the bond lengths of Fe−$\mathbf{N_2}$ (2.154(4) Å) and Fe−$\mathbf{N_5}$ (2.107(4) Å) relative to Fe−$\mathbf{N_3}$ (2.178(4) Å) and Fe−$\mathbf{N_4}$ (2.223(4) Å) correlates with the opposite positioning to the tilt of $\mathbf{Py_1}$. The average value for the five Fe(1)−N(1 → 5) bond lengths (2.162(4) Å) is consistent with the assignment of a *hs* Fe(III) center in this complex.[45,46]

Comparison of the metrical parameters of **1** and **2** indicates that the structures are nearly isostructural (Table 2), even though the metals differ in oxidation state. A RMS error of the structural overlay of the six-coordinated atoms, N(1 → 5) and O(3), and the iron centers of **1** and **2** equals 0.21 Å. The average bond lengths between the iron center in **1** and **2** and $\mathbf{N_{2\rightarrow5}}$ are nearly identical (∼2.16 Å). The two largest structural changes that occur upon oxidation of **1** to **2** are the contraction of the Fe(1)−O(3) bond length from 2.040(3) Å (**1**) to 1.782(3) Å (**2**), and the opening of the Fe(1)−O(3)−C(30) bond angle from 134° (**1**) to 165° (**2**).

Scheme 3

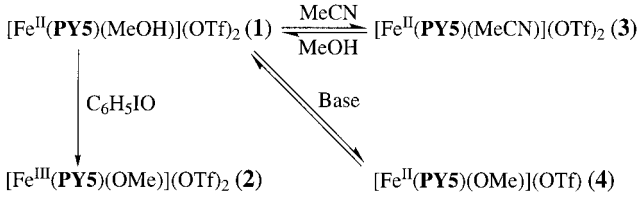

Solution Characterization. The solution behavior of the four iron complexes described in this article is summarized in Scheme 3. The metrical parameters from the solid-state structures of **1** and **2** obtained at 203 K suggest a *hs* ferrous and a *hs* ferric compound, respectively. Solid-state magnetic susceptibility measurements support these assignments (**1**, 298 K, $\mu_{eff} = 5.0\ \mu_B$; **2**, 298 K, $\mu_{eff} = 5.8\ \mu_B$) but also indicate that **1** and **2** undergo cooperative spin-state transitions at ca. 90 K. The ^{1}H NMR spectra of **1** and **2** exhibit features of *hs* complexes with paramagnetically shifted and broadened peaks in the range of −7 to 60 ppm. The peaks assigned to the four protons of each of the pendant pyridyl arms are equivalent, indicating structural equivalence of $\mathbf{Py_{2\rightarrow5}}$ on the NMR time scale for both **1** and **2**. The solution magnetic susceptibility[47] of **1** is equal to 4.7 ± 0.2 BM in MeOH at ambient temperature (RT), slightly less than the anticipated spin-only value of 4.9 μ_B for a *hs* ferrous complex. Variable-temperature solution magnetic sus-

(45) Zang, Y.; Kim, J.; Dong, Y.; Wilkinson, E. C.; Appelman, E. H.; Que, L., Jr. *J. Am. Chem. Soc.* **1997**, *119*, 4197−4205.
(46) Kojima, T.; Leising, R. A.; Yan, S.; Que, L., Jr. *J. Am. Chem. Soc.* **1993**, *115*, 11328−11335.
(47) Evans, D. F. *J. Chem. Soc.* **1959**, 2003−2005.

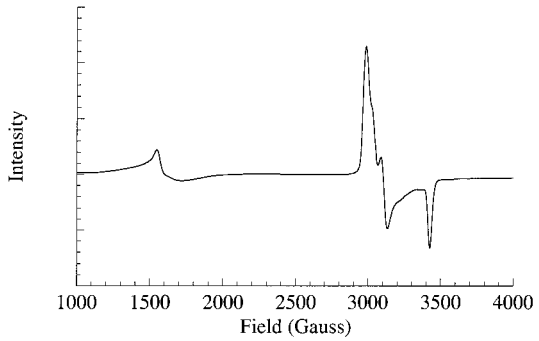

Figure 3. X-band EPR spectrum of [Fe(**PY5**)(OMe)](OTf)$_2$ (**2**) in MeOH at 77 K.

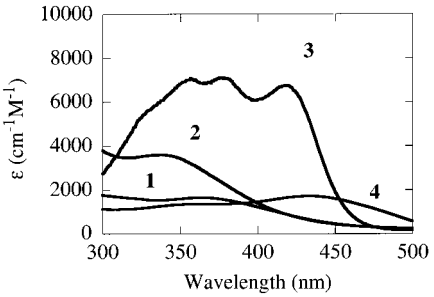

Figure 4. UV/vis spectra of [Fe(**PY5**)(MeOH)](OTf)$_2$ (**1**), [Fe(**PY5**)(OMe)](OTf)$_2$ (**2**), [Fe(**PY5**)(MeCN)](OTf)$_2$ (**3**), and [Fe(**PY5**)(OMe)](OTf) (**4**), all in MeOH, except for **3**, which was taken in MeCN.

ceptibility measurements of **1** show that μ_{eff} decreases to $3.3 \pm 0.2\ \mu_B$ at 191 K, behavior associated with spin transition compounds in solution.[48] The solid-state μ_{eff} of $5.0\ \mu_B$ for the solid at RT suggests that **1** exists as an equilibrium mixture of *hs* and low-spin (*ls*) states in solution.[49] The μ_{eff} of **2** shows similar temperature-dependent susceptibility in MeOH, decreasing from 5.3 ± 0.2 BM at 291 K to 4.4 ± 0.2 BM at 203 K.[49] Fitting the variable-temperature magnetic susceptibility values of **1** and **2** to a *ls*−*hs* equilibrium Boltzmann model gives the following thermodynamic parameters for the transition from *ls* to *hs*: **1**, $\Delta H^\circ = 2.4 \pm 0.2$ kcal mol^{-1}, $\Delta S^\circ = 14.0 \pm 0.5$ eu; **2**, $\Delta H^\circ = 2.2 \pm 0.2$ kcal mol^{-1}, $\Delta S^\circ = 12.2 \pm 0.5$ eu. These values are within the range previously observed for Fe(II)[48,50] and Fe(III)[51,52] spin transition complexes.

The EPR spectrum of **2** in dry MeOH at 77 K is consistent with a mixture of *hs* and *ls* ferric complexes and corroborates the observed solution magnetic susceptibility data (vide supra). The high-field region is tentatively modeled as a rhombic $S = {}^1/_2$ octahedral Fe(III) center with signals at $g = 2.25$, 2.16, and 1.96 (Figure 3). The smaller feature at 1500 G ($g = 4.3$) is consistent with the *hs* component of **2**. The EPR spectrum in nondried MeOH contains more than a single rhombic component.

Solutions of **2** in MeOH, MeCN, and acetone are light orange and are aerobically stable at RT. The UV/vis absorption spectrum in MeOH shows a high-energy feature at 337 nm ($\epsilon = 3600$ M^{-1} cm^{-1}) that likely results from a ligand-to-metal charge transfer (LMCT) transition between the pyridine ligands of **PY5** and the Fe(III) center (Figure 4). Solutions of **1** in MeOH are green-yellow and are aerobically stable for days at RT. The UV/vis spectrum of **1** shows a high-energy feature at 370 nm ($\epsilon = 1650$ M^{-1} cm^{-1}) that is similar in terms of both energy and intensity to other complexes with *hs* Fe(II)−pyridine bonds (Figure 4).[53,54] This band is tentatively assigned as a pyridine MLCT band.[55] Titration of **1** with a strong base shows clean isobestic conversion to a novel complex **4**. The shift to a lower energy band from **1** to **4** is consistent with improved σ-bonding of the exogenous ligand (Figure 4). The conversion of the axial MeOH ligand to a methoxide could account for this behavior; consequently, the novel complex **4** is postulated to be [Fe^{II}(**PY5**)(OMe)](OTf). This complex is stable under anaerobic conditions for hours at RT.

[Fe^{III}(**PY5**)(OMe)](OTf)$_2$ and [Fe^{II}(**PY5**)(OMe)](OTf) differ by a single electron, suggesting that the reduction potential of **2** should be equal to the oxidation of potential of **4**. This redox potential is necessary for the thermodynamic analysis of the reactivity of **2** (vide infra). An irreversible reduction peak at +0.71 V (vs SHE; Fc/Fc$^+$ (MeOH) = +0.610 V vs SHE)[56] is found for **2** in MeOH, while **4** shows an irreversible oxidation peak at +0.76 V ($\Delta E = 0.100$ V). These two potentials differ by ∼50 mV, a difference potentially attributable to the differences of the electrochemical solutions. Due to its limited stability, **4** was generated in situ from **1** by addition of a slight excess of triethylamine. Attempts to perform electrochemistry on **2** with a similar amount of triethylamine immediately decomposed the ferric complex. Given the small difference between these experimental values, the average, +0.73 V, is taken as the reduction potential of **2**. [Fe^{II}(**PY5**)(MeOH)](OTf)$_2$ shows a highly irreversible oxidation potential approximately 200 mV greater than that for **4** (at 0.93 V).

Thermodynamic Justification for Potential Hydrogen Atom Abstraction. Structurally and electronically, complexes **1** and **2** differ only by the net addition of a single hydrogen atom. Based on enthalpic considerations, a bimolecular reaction of **2** with a substrate containing a weak C−H bond may proceed via hydrogen atom abstraction (HA) if the bond strength of the O−H bond created in **1** is greater than or approximately equal to the bond strength of the C−H bond broken. However, an enthalpically unfavored reaction can also proceed to completion if a second fast irreversible process follows the initial HA, such as a radical coupling reaction or a fast secondary oxidation. The O−H bond strength of the ligated MeOH in the product, **1**, can be calculated from a thermodynamic cycle (Scheme 4) that includes the reduction potential of **2** ($E_{red} = 0.73$ V) and the proton affinity of **1** ($pK_a = 9.1 \pm 0.2$) in MeOH.[57] The last two equations in Scheme 4, which describe the free energy of formation of a hydrogen atom and its solvation in MeOH, complete the thermodynamic cycle. As the solvation of a proton in MeOH and that of a proton in H_2O differ, the standard reduction potential of H_2 in MeOH can be calculated using the

(48) Gutlich, P.; Hauser, A.; Spiering, H. *Angew. Chem., Int. Ed. Engl.* **1994**, *33*, 2024−2054.
(49) See Supporting Information.
(50) Chang, H.-R.; McCusker, J. K.; Toftlund, H.; Wilson, S. R.; Trautwein, A. X.; Winkler, H.; Hendrickson, D. N. *J. Am. Chem. Soc.* **1990**, *112*, 6814−6827.
(51) Neya, S.; Tsubaki, M.; Hori, H.; Yonetani, T.; Funasaki, N. *Inorg. Chem.* **2001**, *40*, 1220−1225.
(52) Beattie, J. K.; Binstead, R. A.; Dewey, T. G.; Turner, D. H. *J. Am. Chem. Soc.* **1980**, *102*, 6442−6451.
(53) Hagen, K. S.; Diebold, A. *Inorg. Chem.* **1998**, *37*, 215−223.
(54) Que, L., Jr. In *Iron Carriers and Iron Proteins*; Loehr, T. M., Ed.; VCH Publishing: New York, 1989; pp 467−524.
(55) Borovik, A. S.; Papaefthymiou, V.; Taylor, L. F.; Anderson, O. P.; Que, L., Jr. *J. Am. Chem. Soc.* **1989**, *111*, 6183−6195.
(56) Zuman, P.; Meites, L. *Electrochemical Data*; John Wiley & Sons: New York, 1974; Vol. A.
(57) The calculated pK_a differs slightly from that previously reported in ref 35.

Scheme 4

		Energy (kcal mol^{-1})
$[Fe^{II}(\mathbf{PY5})(MeOH)]^{2+}$ (g)	$\longrightarrow$ $[Fe^{II}(\mathbf{PY5})(MeOH)]^{2+}$ (me)	ΔG^1_{solv} [a]
$[Fe^{II}(\mathbf{PY5})(MeOH)]^{2+}$ (me)	$\longrightarrow$ $[Fe^{II}(\mathbf{PY5})(OMe)]^{2+}$ (me) + H^+ (me) $(pK_a = 9.1)$	12.4
$[Fe^{II}(\mathbf{PY5})(OMe)]^{2+}$ (me)	$\longrightarrow$ $[Fe^{III}(\mathbf{PY5})(OMe)]^{2+}$ (me) + e^- $(E_{pc} = 0.730$ V$)$	16.8
$[Fe^{III}(\mathbf{PY5})(OMe)]^{2+}$ (me)	$\longrightarrow$ $[Fe^{III}(\mathbf{PY5})(OMe)]^{2+}$ (g)	$-\Delta G^2_{solv}$ [a]
H^+ (me) + e^-	$\longrightarrow$ $^1/_2$ H_2 (g)	C [b]
$^1/_2$ H_2 (g)	$\longrightarrow$ $H^\bullet$ (g)	
$[Fe^{II}(\mathbf{PY5})(MeOH)]^{2+}$ (g)	$\longrightarrow$ $[Fe^{III}(\mathbf{PY5})(OMe)]^{2+}$ (g) + $H^\bullet$ (g)	**83.5**

[a] ΔG^1_{solv} assumed to be equal to ΔG^2_{solv}. [b] This constant contains the entropic free energy associated with the solvation of a hydrogen atom. Subtraction of this term from the sum of the free energies above gives the resulting enthalpic bond dissociation energy. [c] Species followed by the notation (*me*) are in MeOH solution.

known energy of the $H_{2(g)}/H^+_{(MeOH)}$ couple relative to the hydrogen electrode in water.[58] The H_2 reduction potential, the H_2 bond dissociation energy (BDE), and the entropic contribution at 298 K are conveniently combined into a single constant *C*,[59] and equal 54.4 kcal mol^{-1}. The energy calculation for the overall reaction is an enthalpic BDE.

An independent check of the value of *C* in MeOH can be determined from any chemical with a known pK_a in MeOH, a well-defined oxidation potential for its conjugate base in MeOH, and a known BDE. Phenol is a convenient reference; BDE = 88.6 kcal mol^{-1},[60,61] pK_a(MeOH) = 14.3.[62] Using an experimentally determined oxidation potential of the phenolate anion in MeOH (E_{red} = 0.640 V vs SHE), the value of *C* calculated from the phenol reference is nearly identical (54.4 kcal mol^{-1}) to the first value. By both methods, the O−H bond strength of the MeOH ligand in **1** is calculated as 83.5 ± 2.0 kcal mol^{-1}. This O−H BDE is dramatically reduced relative to that of unligated MeOH (102 kcal mol^{-1}).[63]

Oxidation of 2,4,6-Tri-*tert*-butylphenol. The ability of **2** to formally remove a hydrogen atom was initially probed by using 2,4,6-tri-*tert*-butylphenol (TTBP) as a substrate. The TTBP radical is relatively stable in MeOH ($t_{1/2}$ = 1 h) and is readily identifiable due to its strong UV/vis absorption bands.[64] Additionally, TTBP has a relatively weak O−H bond of 81 kcal mol^{-1}.[61] The weak O−H BDE combined with the faster reaction of phenols relative to C−H substrates of similar BDE[65] makes a formal hydrogen atom transfer rapid compared to the normal radical decay, allowing a measurable amount of the radical to form in solution. The reaction of 10 equiv of TTBP with **2** in MeOH under N_2 at RT generates the characteristic blue-green color of the TTBP radical. EPR analysis at 77 K of the reaction aliquots shows rapid decay of the ferric species followed by the growth of the TTBP radical, g = 2 signal. However, the radical intensity develops only after most of **2** is consumed, implicating a fast secondary reaction of the phenoxyl radical with a second equivalent of **2**. Quantitation of the EPR signal indicates that a substoichiometric amount of TTBP radical is formed, but this reaction clearly indicates that **2** can react through a formal hydrogen atom transfer reaction.

Quantifying the rate of reduction of **2** by optical spectroscopy is faciliated in MeCN, as the product **3** has much more intense MLCT bands than **1**. At 298 K, the anaerobic decay of **2** in MeCN follows clean first-order kinetics under conditions of excess TTBP (>40 equiv), with the rate constant linearly dependent on the concentration TTBP. A calculated second-order rate constant is k_2 = 0.60 ± 0.05 M^{-1} s^{-1}. The slower reactivity with TTBP deuterated in the phenolic position (k_2 = 0.30 ± 0.05 M^{-1} s^{-1}) gives a kinetic isotope effect of 2.0, suggesting that O−H(D) bond cleavage is involved in the rate-determining step.

Oxidation of Cyclohexadiene. The reaction of **2** with substrates containing weak C−H bonds under N_2 results in the reduction of the Fe(III) center and oxidation of the substrates. The nature of the mechanism of substrate activation is of obvious interest, given the structural similarities of **2** and activated LO. Natural substrates of LOs, such as linoleic acid and arachidonic acid, contain a *cis*,*cis*-1,4-pentadiene subunit where stereospecific C−H bond cleavage is proposed to occur. A minimal substrate model for the *cis*,*cis*-1,4-pentadiene subunit is 1,4-cyclohexadiene (CHD), which has a C−H BDE of 75 ± 4 kcal mol^{-1}.[66,67] CHD slowly reduces **2** to **1** in MeOH, as monitored by UV/vis spectroscopy. If the reaction occurs in MeCN, the reduced product, **1**, immediately undergoes solvent exchange to form *ls* $[Fe^{II}(\mathbf{PY5})(MeCN)](OTf)_2$ (**3**), as indicated by its diamagnetic ^{1}H NMR spectrum and the increased intensity and shifting of the MLCT band (Figure 4). $[Fe^{II}(\mathbf{PY5})(MeCN)](ClO_4)_2$ has been previously characterized.[36] In MeCN solution, **3** is indefinitely stable, and the vastly different UV/vis spectra of **2** and **3** facilitate the monitoring of these reactions. The progress of the reaction can also be monitored by ^{1}H NMR. ^{1}H NMR analysis of the organic products shows 0.5 equiv of benzene produced for each equivalent of the ferric complex reduced (>95%). As measured optically in both MeOH and MeCN at 298 K, the anaerobic decay of **2** follows first-order kinetics under conditions of excess substrate with the rate constant linearly dependent on the concentration of the substrate

(58) Johnsson, M.; Persson, I. *Inorg. Chim. Acta* **1987**, *127*, 15−24.
(59) Bordwell, F. G.; Cheng, J. P.; Harrelson, J. A., Jr. *J. Am. Chem. Soc.* **1988**, *110*, 1229−1231.
(60) DosSantos, R. M. B.; Simoes, J. A. M. *J. Phys. Chem. Ref. Data* **1998**, *27*, 707−739.
(61) Pedulli, G. F.; Lucarini, M.; Pedrielli, P.; Cabiddu, S.; Fattuoni, C. *J. Org. Chem.* **1996**, *61*, 9259−9263.
(62) *Lange's Handbook of Chemistry*, 14th ed.; Dean, J. A., Ed.; McGraw-Hill: New York, 1992.
(63) Kerr, J. A. *Chem. Rev.* **1966**, *66*, 465−500.
(64) Cook, C. D.; Kuhn, D. A.; Fianu, P. *J. Am. Chem. Soc.* **1955**, *78*, 2002−2005.
(65) Lockwood, M. A.; Blubaugh, T. J.; Collier, A. M.; Lovell, S.; Mayer, J. M. *Angew. Chem., Int. Ed.* **1999**, *38*, 225−227.
(66) Mulder, P.; Laarhoven, L. J. J.; Wayner, D. D. M. *Acc. Chem. Res.* **1999**, *32*, 342−349.
(67) Burkey, T. J.; Majewski, M.; Griller, D. *J. Am. Chem. Soc.* **1986**, *108*, 2218−2221.

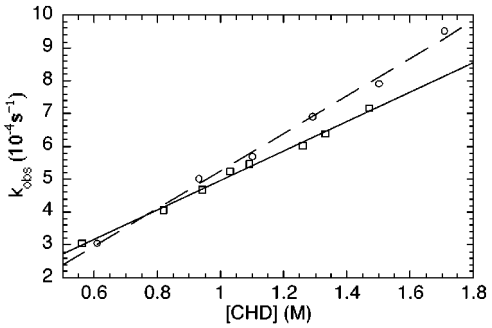

Figure 5. First-order rate constants for the reduction of [Fe^{III}(**PY5**)(OMe)](OTf)$_2$ (**2**) to **1** in the presence of 1,4-cyclohexadiene in MeOH (□) and MeCN (○). All data taken with greater than 40-fold excess of cyclohexadiene under anaerobic conditions at 298 K. k_{2corr}(MeCN) = 2.8×10^{-4} M^{-1} s^{-1}, k_{2corr}(MeOH) = 2.4×10^{-4} M^{-1} s^{-1}.

Scheme 5

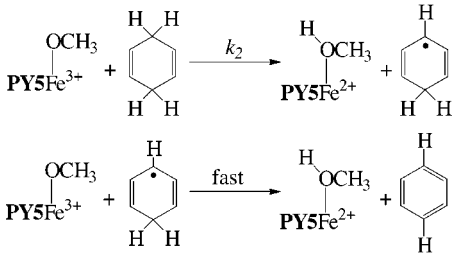

(Figure 5). The observed rate constant does not change as the concentration of **2** is systematically varied between 0.16 mM and 0.23 mM with 0.066 M fluorene, suggestive of a first-order dependence on **2** and an overall second-order rate law (eq 3). The second-order rate constants need to be statistically

$$\frac{d[Fe^{II}(\mathbf{PY5})(MeOH)^{2+}]}{dt} = k_2[Fe^{III}(\mathbf{PY5})(OMe)^{2+}][CHD] \quad (3)$$

corrected for the number of weak C−H bonds (e.g., CHD has four equivalent weak C−H bonds) and for secondary reactions: k_{2corr}(MeOH) = (2.4 ± 0.2) × 10^{-4} M^{-1} s^{-1}, k_{2corr}(MeCN) = (2.8 ± 0.4) × 10^{-4} M^{-1} s^{-1}, 298 K. The per-deuterated analogue of CHD (CHD-d_8) reacts at a significantly reduced rate relative to CHD: k_{2corr}(MeOH) = (9.0 ± 0.3) × 10^{-5} M^{-1} s^{-1}, k_{2corr}(MeCN) = (8.0 ± 0.3) × 10^{-5} M^{-1} s^{-1}, 298 K. The ratios of the rate constants ($k_{CHD}/k_{CHD\text{-}d_8}$) are 2.7 and 3.4 in MeOH and MeCN, respectively, suggestive of a primary KIE for the observed reactivity.

The combination of a second-order rate law and a primary KIE using deuterated substrates indicates that the reduction of **2** is most easily understood as a bimolecular process in which C−H bond cleavage is the rate-determining step. The collision of **2** with a weak C−H group on CHD results in 1 equiv of **1** and a CHD substrate radical (Scheme 5). A fast secondary reaction is proposed to follow, as the C−H BDE of the radical is thought to be significantly reduced from that of CHD, and the radical is quenched with a further equivalent of **2**. As a test for the presence of radicals, the reactions were run in the presence of O_2. Because O_2 is known to react with radicals near the diffusion limit,[68] it should compete with **2** for CHD radicals. Indeed, the decay rate of **2** for the reactions under O_2 is ∼2-fold slower than that measured under O_2-free conditions, with a slightly greater effect in MeOH as compared to that in MeCN.

If the hydrogen-transfer reaction proceeds via a charged species, then the observed rate constants would be expected to be orders of magnitude different in protic versus aprotic solvents.[69] The similarity of k_{2corr} in MeOH and MeCN for CHD supports a radical-based process. The consistent kinetic behavior of the reduction of **2** in both MeOH and MeCN and the perturbation of reaction rate in the presence of O_2 support a rate-limiting HA step in the oxidation process.

Table 3. Second-Order Rate Constants for the Reactions of Hydrocarbon Substrates with [Fe^{III}(**PY5**)(OMe)](OTf)$_2$ (**2**) in MeOH and MeCN

substrate	k_{2corr}(MeOH)[a]	k_{2corr}(CH_3CN)[a]	KIE[b]
toluene	(1.5 ± 0.4) × 10^{-4}	(1.9 ± 0.4) × 10^{-4}	6.5
ethylbenzene	(2.3 ± 0.3) × 10^{-4}	(2.3 ± 0.2) × 10^{-4}	–
2,3-dimethyl-2-butene	(2.8 ± 0.2) × 10^{-4}	(3.0 ± 0.3) × 10^{-4}	–
4-methyl-1,3-pentadiene	(2.3 ± 0.6) × 10^{-3}	(2.1 ± 0.5) × 10^{-3}	–
9,10-dihydroanthracene	(4.9 ± 0.3) × 10^{-3}	(5.0 ± 0.1) × 10^{-3}	5.5
1,4-cyclohexadiene	(2.7 ± 0.4) × 10^{-2}	(3.0 ± 0.4) × 10^{-2}	2.7

[a] Second-order rate constants per available C−H bond were measured at 323 K in units of M^{-1} s^{-1} and were adjusted for reaction stoichiometry to yield k_{2corr}. [b] Kinetic isotope effect determined in MeOH at 298 K.

Other Hydrocarbon Substrate Reactivity. The linear correlation of the log of the C−H bond cleavage reaction rate constants with C−H BDE has been established for a number of metal−oxo complexes, including chromyl chloride and permanganate species.[28−31,70] This empirical correlation between the activation energy (E_a) and the enthalpic driving force (ΔH) is consistent for primary, secondary, and tertiary C−H bonds and appears to be independent of substrate spatial demands. The Evans−Polanyi relationship suggests that in HA reactions, the entropies of C−H bond activation are essentially constant, resulting in a linear relationship between log(k_{2corr}) and ΔH.[71,72] Thus, at parity of substrate, the primary determinant of HA reactivity for a metal−oxo complex is the strength of the O−H bond created.

Further support for a HA mechanism in the reduction of **2** by CHD results from the reactivity profiles of other substrates containing weak C−H bonds with **2**. Because the reaction rates are slow at 298 K, the reactions were performed at 323 K in both MeOH and MeCN. Under pseudo-first-order conditions of substrate, the reduction of **2** was examined using the following substrates: toluene, ethylbenzene, 2,3-dimethyl-2-butene, 4-methyl-1,3-pentadiene, 9,10-dihydroanthracene (DHAn), 1,4-cyclohexadiene, xanthene, fluorene, tetralin, diphenylmethane, triphenylmethane, and cumene. The first six substrates were analyzed in both MeOH and MeCN, while the last five were analyzed only in MeCN. As with CHD at 298 K, all substrates examined in MeOH and MeCN exhibit similar rates in both protic and aprotic solutions (Table 3). In addition, the deuterated analogues toluene-d_8 and 9,10-dihydroanthracene-d_4 were examined in MeOH to assess the nature of the rate-limiting step. Oxidations of both deuterated analogues were significantly slower than for the nondeuterated substrates,

(68) Maillard, B.; Ingold, K. U.; Scaiano, J. C. *J. Am. Chem. Soc.* **1983**, *105*, 5095−5099.
(69) Avila, D. V.; Brown, C. E.; Ingold, K. U.; Lusztyk, J. *J. Am. Chem. Soc.* **1993**, *115*, 466−470.
(70) Mayer, J. M.; Wang, K. *J. Am. Chem. Soc.* **1997**, *119*, 1470−1471.
(71) Tedder, J. M. *Angew. Chem., Int. Ed. Engl.* **1982**, *21*, 401−410.
(72) Ingold, K. U.; Russel, G. A. In *Free Radicals*; Kochi, J. K., Ed.; Wiley: New York, 1973; pp 283−293.

Table 4. Corrected Second-Order Rate Constants for the Reactions of Hydrocarbon Substrates with [Fe^{III}(**PY5**)(OMe)](OTf)$_2$ (**2**) in MeCN

substrate	$k_{2corr}(CH_3CN)$[a]	BDE[b]	ref[c]	$\Delta H°$ [d]
toluene	$(1.9 \pm 0.4) \times 10^{-4}$	88 ± 1	108	+4.5
ethylbenzene	$(2.3 \pm 0.2) \times 10^{-4}$	85 ± 1	93, 109	+1.5
tetralin	$(2.9 \pm 0.2) \times 10^{-4}$	85 ± 1	109	+1.5
cumene	$(9.5 \pm 0.4) \times 10^{-3}$	83 ± 1	109	−0.5
2,3-dimethyl-2-butene	$(3.0 \pm 0.3) \times 10^{-4}$	82 ± 2	110, 111	−1.5
diphenylmethane	$(8.9 \pm 0.4) \times 10^{-4}$	82 ± 1	107, 113	−1.5
triphenylmethane	$(1.8 \pm 0.4) \times 10^{-3}$	81 ± 1	107	−2.5
4-methyl-1,3-pentadiene	$(2.1 \pm 0.5) \times 10^{-3}$	81 ± 2	93, 114	−2.5
fluorene	$(3.3 \pm 0.2) \times 10^{-3}$	80 ± 2	107, 112	−3.5
9,10-dihydroanthracene	$(5.0 \pm 0.1) \times 10^{-3}$	78 ± 2	107	−5.5
1,4-cyclohexadiene	$(3.0 \pm 0.4) \times 10^{-2}$	75 ± 4	66, 67	−8.5
xanthene	$(2.8 \pm 0.2) \times 10^{-2}$	75 ± 1	112	−8.5

[a] Second-order rate constants per available C−H bond were measured at 323 K in units of M^{-1} s^{-1} and were adjusted for reaction stoichiometry. [b] For the weak C−H bond in units of kcal mol^{-1}. [c] References are for literature BDE of substrates. [d] Relative to the bond dissociation energy of the O−H bond in the bound MeOH in **1** (83.5 kcal mol^{-1}).

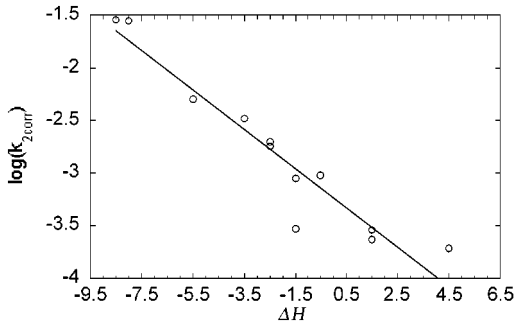

Figure 6. Dependence of the k_{2corr} of the reduction of [Fe^{III}(**PY5**)(OMe)](OTf)$_2$ (**2**) on ΔH. All data taken with greater than 40-fold excess of substrate under anaerobic conditions in MeCN at 323 K. ΔH is relative to 83.5 kcal mol^{-1}, the bond dissociation energy of the O−H bond in the bound MeOH in **1**.

with $k_{C_{14}H_{12}}/k_{C_{14}H_8D_4} = 5.5 \pm 0.5$ for DHAn and $k_{C_7H_8}/k_{C_7D_8} = 6.5 \pm 1$ for toluene in MeOH at 298 K.

A plot of log(k_{2corr}) versus the pK_a of each substrate[49] does not show a linear relationship, as is found between log(k_{2corr}) and the C−H bond BDE (Table 4) of each substrate. This latter linear relationship supports a HA mechanism and is graphically presented as a plot of log(k_{2corr}) versus $\Delta H°$ of the reaction (Figure 6), where $\Delta H°$ is defined as the strength of the O−H bond in **1** subtracted from the C−H BDE of each substrate. The correlation appears unaffected by steric crowding within each substrate, as evidenced by the normal reactivity of extremely bulky substrates such as triphenylmethane.

Discussion

Modeling of metalloenzymes provides the opportunity to create not only spectroscopic and structural models of an active site but also functional analogues. The ability to systematically vary the coordination sphere with a synthetic model is a powerful probe for elucidating the role of the ligation sphere in conferring specific reactivity to a metal site. The ligand **PY5** most closely resembles the coordination sphere of mammalian lipoxygenases (LO) that contain four imidazoles from histidines and one carboxylate; certainly, a better model would include a carboxylate ligand and less π-back-bonding nitrogenous ligands to better simulate imidazole ligation. However, several essential features of the endogenous ligation sphere of LO are effectively reproduced. The pentadentate **PY5** ligand enforces a square pyramidal endogenous ligation of the enzyme that leaves an exogenous ligand site similar to the enzyme. Additionally, the endogenous ligands of both the synthetic complex and the enzyme are relatively uncharged, enabling very positive reduction potentials for the ferric complexes (vide supra). Both the structure and the reactivity of [Fe^{II}(**PY5**)(MeOH)](OTf)$_2$ (**1**) and [Fe^{III}(**PY5**)(OMe)](OTf)$_2$ (**2**) suggest that **PY5** creates a reasonable model for LO by simple mimicry of the coordination site of the enzyme.

The most dramatic structural similarity between the model complexes and LO is the short Fe(1)−O(3) distance observed in the crystal structure of **2**; this distance is reminiscent of the short Fe−O distance (1.88 Å) observed in the EXAFS information for the proposed ferric−hydroxide species in activated LO.[13] Both the Fe(1)−O(3) bond length (1.782(3) Å) and the Fe(1)−O(3)−C(30) bond angle (165°) in **2** are near the extremes for terminally bound methoxide anions in structurally characterized iron complexes.[39,73,74] These metrical parameters are generally associated with more electron-deficient metals such as titanium[75−77] and zirconium.[78] The neutral **PY5** ligation to the Fe(III) center generates an extremely Lewis-acidic metal site that reduces its electron deficiency by π-bonding to the lone pair electrons of the exogenous methoxide ligand. This multiple-bond character for the Fe−OMe bond is similar to that proposed to occur for the oxide bridge in μ-oxo−ferric dimer complexes.[39,79] The π and σ-bonding effects and negative charge of the methoxide ligand in **2** are thought to be important in the stabilization of this higher oxidation state. As a result of the multiple-bond character, the Fe(1)−O(3) bond contracts significantly. The proposed hydroxide ligand in the ferric active form of LO shows a similar Fe(III)−O contraction from the ferrous−H_2O form and may act in an analogous manner to stabilize the ferric active species.[14,80,81]

Electronically, **2** also resembles LOs. The crystal structure and both solid-state and solution magnetic susceptibility measurements show that **2** is predominantly high-spin at 298 K, as are the ferric sites of SLO-1 and 5-human lipoxygenase (5-HLO).[82,83] The LOs differ from **2** in that the native enzymes do not exhibit spin-crossover behavior. The electrochemical behavior of **2** is also similar to that of LO. The redox potential of **2** at ~0.73 V is in the same range as that measured for SLO-1 (0.6 ± 0.1 V vs SHE).[1] These potentials are much higher than that of the simplest ferric model complex of

(73) Lecomte, C.; Chadwick, D. L.; Coppens, P.; Stevens, E. D. *Inorg. Chem.* **1983**, *22*, 2982−2992.
(74) Hoard, J. L.; Hamor, M. J.; Hamor, T. A.; Caughey, W. S. *J. Am. Chem. Soc.* **1965**, *87*, 2312−2319.
(75) Aslan, H.; Sielisch, T.; Fischer, R. D. *J. Organomet. Chem.* **1986**, *315*, C69−C72.
(76) Boreham, C. J.; Buisson, G.; Duee, E.; Jordanov, J.; Latour, J.-M.; Marchon, J.-C. *Inorg. Chim. Acta* **1983**, *70*, 77−82.
(77) Wright, D. A.; Williams, D. A. *Acta Crystallogr., Sect. B* **1968**, *24*, 1107−1114.
(78) Karia, R.; Willey, G. R.; Drew, M. G. B. *J. Chem. Soc., Dalton Trans.* **1986**, 2493−2495.
(79) Holm, R. H. *Chem. Rev.* **1987**, *87*, 1401−1449.
(80) Zhang, Y.; Gebhard, M. S.; Solomon, E. I. *J. Am. Chem. Soc.* **1991**, *113*, 5162−5175.
(81) Deaton, J. C.; Gebhard, M. S.; Solomon, E. I. *Inorg. Chem.* **1989**, *28*, 877−889.
(82) Cheesbrough, T. M.; Axelrod, B. *Biochemistry* **1983**, *22*, 3837−3840.
(83) Chasteen, N. D.; Grady, J. K.; Skorey, K. I.; Neden, K. J.; Riendeau, D.; Percival, M. D. *Biochemistry* **1993**, *32*, 9763−9771.

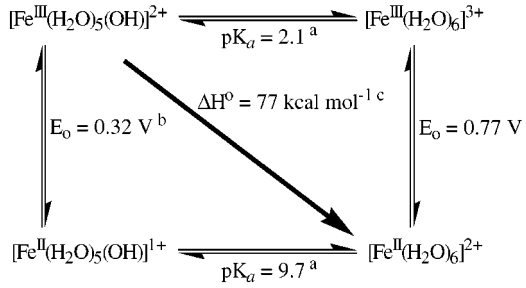

Figure 7. Thermodynamic cycle for the $[Fe^{III}(H_2O)_5(OH)]^{2+}/[Fe^{II}(H_2O)_6]^{2+}$ system in H_2O. [a]From ref 85. [b]Calculated from the above literature values. [c]Calculated from the equation BDE = 1.37 pK_{HA} + 23.06$E_o(A^-)$ + C, with a C value of 56.[115]

LO, namely the monodeprotonated ferric hexaaquo complex, $[Fe^{III}(H_2O)_5(OH)]^{2+}$ (0.32 V vs SHE, Figure 7).

The pK_a of **1** in MeOH is 9.1 ± 0.2, while the estimated pK_a for the ferrous−H_2O form of human LO is >10.[84] For comparison, $[Fe^{II}(H_2O)_6]^{2+}$ has a pK_a of 9.7.[85] The very positive reduction potential of **2** combined with the basicity of the methoxide ligand of **4** allows the methoxide ligand of **2** to be a suitable model for the proposed hydroxide ligand in the active native species. A thermodynamic analysis shows that the conversion of **2** to **1** in MeOH results in the formation of an O−H bond with a bond dissociation energy (BDE) of 83.5 ± 2.0 kcal mol^{-1}. A similar analysis of the O−H BDE in the ferrous−H_2O form of LO and $[Fe^{II}(H_2O)_6]^{2+}$ gives 85 and 77 kcal mol^{-1}, respectively.[86]

In the proposed mechanism of LO, the ferric−hydroxide species cleaves a substrate C−H bond via HA with concomitant reduction of the active site to a ferrous−water species (Scheme 2); **2** appears to react with substrates in an analogous manner. 2,4,6-Tri-*tert*-butylphenol (TTBP) reduces **2** to generate a tri-*tert*-butylphenoxyl radical, demonstrating the ability of **2** to formally accept a hydrogen atom. However, this reactivity does not distinguish between a concerted hydrogen atom transfer mechanism and other mechanisms consisting of discrete proton and outer-sphere electron-transfer steps. An inner-sphere mechanism involving a ferric 2,4,6-tri-*tert*-butylphenoxide complex is unlikely, given that there are no structurally characterized octahedral metal complexes that include a 2,6-disubstituted *tert*-butylphenoxide ligand.[87,88] The observed kinetic isotope effect (KIE) of 2.0 ± 0.3 for the reduction of **2** by TTBP is large for a secondary isotope effect, particularly given that the KIE for TTBP proton self-exchange is 1.24,[89] and suggests that C−H bond cleavage may be involved in the RDS. In addition, the observation of large primary KIEs for cyclohexadiene, dihydroanthracene (DHAn), and toluene implicates C−H cleavage in the RDS for the reduction of **2** by hydrocarbons.

Two likely alternative mechanisms consistent with the rate-determining O−H or C−H bond cleavage are either fast electron transfer followed by a rate-limiting proton abstraction, or a rate-limiting proton abstraction followed by fast electron transfer. The fast rate of the reduction of **2** by TTBP in MeCN (k_2 = 0.60 M^{-1} s^{-1}) precludes the former mechanism of fast electron transfer as an initial step. The high oxidation potential of TTBP (1.60 V vs SHE in MeCN)[90] along with the positive reduction potential of **2** predicts an intermediate with $\Delta G°$ = 19.8 kcal mol^{-1}, a free energy higher than that of the empirical transition state ($\Delta G^‡$ = 17.5 kcal mol^{-1}). Similar analysis of the reactivity of **2** with DHAn (vide supra) precludes fast initial electron transfer for hydrocarbons. Using a lower limit estimate $E°$ of ~2.0 V vs SHE for the oxidation potential of DHAn,[91] an initial outer-sphere oxidation of DHAn by **2** would be ca. 1.3 V uphill ($\Delta G°$ = 30 kcal mol^{-1}), much higher than the observed $\Delta G^‡$ of 20.8 kcal mol^{-1} at 298 K. Analysis of the reactivity of **2** with a series of hydrocarbons provides evidence against a slow initial proton transfer as a mechanistic step. In all cases, the rate is first-order with respect to both the concentration of **2** and the concentration of substrate. The empirical second-order rate constants, corrected for the number of weak C−H bonds in the substrate and the reaction stoichiometry, yield an adjusted second-order rate constant, k_{2corr}. The nonlinear relation between log(k_{2corr}) and the pK_a[49] precludes initial proton abstraction as a rate-limiting step.

The elimination of the likely alternative mechanisms leaves HA as the probable mechanistic pathway. Evidence for HA as a mechanistic pathway includes the similar rates of reaction in MeOH and MeCN, suggesting that the reactions progress without change in the charge distribution. The most convincing argument for HA over other potential mechanisms is the strongly linear relationship between log(k_{2corr}) and the substrate's C−H BDE.

Given this linear relationship, an unknown C−H BDE of a substrate that reduces **2** can be measured using an empirically determined reaction rate. The LO substrate, linoleic acid, contains a *cis*,*cis*-1,4-pentadiene subunit where stereospecific C−H bond cleavage takes place. The bond dissociation energy (BDE) for the weak C−H bond of 1,4-pentadiene is found to be 77 kcal mol^{-1} when the molecule adopts a planar conformation.[92,93] The geometric constraints of a *cis*,*cis*-diene fatty acid effectively preclude the formation of a planar 1,4-pentadiene subunit and will certainly increase the C−H BDE of linoleic acid above 77 kcal mol^{-1}.[94] The anaerobic reaction of excess ethyl linoleate, the ester-protected linoleic acid, and **2** produces **1** and several isomeric trienes in a ~50% yield, as identified by GC−MS. The second-order rate constant for C−H bond activation yields k_{2corr} = (9.0 ± 0.5) × 10^{-4} M^{-1} s^{-1}. By comparison with the rates of substrates with calculated and/or experimentally determined BDE values, the C−H bond strength of the C_{11} hydrogen (Scheme 1) is estimated as 83 ± 1 kcal mol^{-1}. This BDE is 6 kcal mol^{-1} greater in energy than the estimated value from 1,4-pentadiene, suggesting that only one of the olefins of linoleic acid significantly conjugates to the radical in the transition state when reacting with **2**. Linoleic acid appears to react with the enzyme in a similar manner. EPR studies show an intermediate organic radical species that is more consistent with delocalization over three, not five, carbon atoms.[1]

(84) Holman, T. R. Personal communication about pK_a of ferrous human LO.
(85) Martell, A. E.; Smith, R. M. *Critical Stability Constants*; Plenum: New York, 1976; Vol. IV, p 1.
(86) Given a C value of 56 kcal mol^{-1} (ref 115).
(87) Darensbourg, D. J.; Zimmer, M. S.; Rainey, P.; Larkins, D. L. *Inorg. Chem.* **1998**, *37*, 2852−2853.
(88) Geerts, R. L.; Huffman, J. C.; Caulton, K. G. *Inorg. Chem.* **1986**, *25*, 1803−1805.
(89) Arick, M. R.; Weissman, S. I. *J. Am. Chem. Soc.* **1968**, *90*, 1654.
(90) Bordwell, F. G.; Cheng, J. P. *J. Am. Chem. Soc.* **1991**, *113*, 1736−1743.
(91) Schlesener, C. J.; Amatore, C.; Kochi, J. K. *J. Am. Chem. Soc.* **1984**, *106*, 3567−3577.
(92) Clark, K. B.; Culshaw, P. N.; Griller, D.; Lossing, F. P.; Simões, J. A. M.; Walton, J. C. *J. Org. Chem.* **1991**, *56*, 5535−5539.
(93) McMillen, D. F.; Golden, D. M. *Annu. Rev. Phys. Chem.* **1982**, *33*, 493−532.
(94) Fort, R. C., Jr.; Hrovat, D. A.; Borden, W. T. *J. Org. Chem.* **1993**, *58*, 211−216.

Table 5. Reaction Parameters for Coordination Complexes' Reactivity with 9,10-Dihydroanthracene via Hydrogen Atom Abstraction[a]

complex	ref	$\Delta H^{\ddagger}$ [b]	$\Delta S^{\ddagger}$ [c]	BDE[d]	ΔH° [e]
$[Fe(Hbim)(H_2bim)_2]^{2+}$	33	11.6	−36	76 ± 2	+2
MnO_4^-	32	13.8	−15	80 ± 3	−2
$[L_2Mn(O)_2MnL_2]^{3+}$	70	14.5	−23	79 ± 2	−1
$[L_2Mn(O)(OH)MnL_2]^{3+}$	70	16.0	−21	75 ± 2	+3
2	this work	13.4	−25	83.5 ± 2	−5.5

[a] Measured in MeCN under anaerobic conditions over the temperature range 298−343 K. [b] Measured in kcal mol^{-1}. [c] Measured in e.u. [d] Energy of the X−H bond formed upon reduction of the metal complex in kcal mol^{-1}. [e] Relative to the BDE of dihydroanthracene (78 kcal mol^{-1}).

Furthermore, SLO-1 can oxygenate monounsaturated fatty acids, albeit at rates much slower than that for the natural substrate, raising the possibility that the role of the second olefinic unit is one of recognition.[95]

Attempts to reproduce the enzymatic catalytic activity with **2** under O_2 to produce alkyl peroxide products are complicated by the lack of a substrate binding site in **2**. In the enzymatic mechanism, the peroxyl radical that results from the reaction of O_2 with the initial alkyl radical abstracts a hydrogen atom from the water attached to the reduced metal center to re-form the oxidized metal site (Scheme 2). In the case of **2**, the intermediate radicals should be free to diffuse from the reduced metal complex **1** before subsequent reaction with O_2 to create the alkyl peroxyl radical. An alkyl peroxyl radical should be a more reactive oxidant than **2**, not only because the O−H BDE of an alkyl peroxide is significantly greater than that of **1** (ca. 90 kcal mol^{-1}, ROOH; 83.5 kcal mol^{-1}, **1**) but also because the reactive oxygen in the alkyl peroxyl radical is less sterically hindered than the methoxide oxygen in **2**. In the presence of excess substrate, the formed alkyl peroxyl radical would likely start a radical chain reaction. Since the products of the metal-based and organic radical-based reactions are identical, the resultant catalytic activity cannot be attributed to turnover at the metal complex as it can for the enzyme.

The HA ability of other simple metal coordination complexes has been determined.[32,33,70] The reaction of 9,10-dihydroanthracene (DHAn) is often used as a standard to gauge relative reactivity since identification of the organic product anthracene is straightforward. Generally, $\log(k_{2corr})$ scales well with ΔH°, particularly in the cases of oxygen-based organic radicals and metal−oxo complexes such as MnO_4^-.[33] A closer inspection of the reactivity, however, reveals that other metal complexes deviate slightly from this correlation. The ferric biimidazole system of Roth and Mayer abstracts hydrogen atoms at about the same rate as $[Fe^{III}(\mathbf{PY5})(OMe)](OTf)_2$, although the N−H bond formed (76 ± 2 kcal mol^{-1}) is roughly 7 kcal mol^{-1} lower.[33]

An Eyring plot analysis of the reaction of **2** with DHAn over the range of 298−343 K[49] indicates a $\Delta H^{\ddagger}$ of 13.4 ± 0.5 kcal mol^{-1} and a $\Delta S^{\ddagger}$ of −25 ± 3 eu. An analysis of the two kinetic parameters and ΔH° for the two iron systems as well as three manganese systems shows little correlation between $\Delta H^{\ddagger}$ and ΔH° (Table 5). $\Delta S^{\ddagger}$ varies independently of ΔH° as well. Consequently, there does not appear to be a simple linear correlation between ΔH° and the rate of HA among the studied coordination complexes as found for simple radicals. One complicating factor may be the differing steric hindrance around the hydrogen abstracting moieties. The methyl moiety of the methoxide ligand and the bulk of the **PY5** ligand, for instance, may make the reactive methoxide oxygen in **2** less accessible than the four unshielded oxygens of MnO_4^-. A second and perhaps more important factor introduced by Mayer and Wang involves the differing structural reorganizational energies for each system affecting the rate of HA.[70]

Summary

A new ligand, 2,6-bis(bis(2-pyridyl)methoxymethane)pyridine (**PY5**), provides the necessary ligation to mimic the five-coordinate endogenous coordination sphere in the iron active site in LOs, more closely resembling the active site of mammalian LOs than plant LOs. An Fe(III) complex of **PY5** with an axial methoxide ligand, $[Fe^{III}(\mathbf{PY5})(OMe)](OTf)_2$ (**2**), was synthesized from the oxidation of $[Fe^{II}(\mathbf{PY5})(MeOH)](OTf)_2$ (**1**) with H_2O_2 or iodosobenzene. The ferric complex shares many of the structural and spectroscopic attributes of native LO. In the most widely accepted mechanism for the function of LOs, the rate-limiting step involves abstraction of a hydrogen atom from the *cis*,*cis*-1,4-pentadiene subunit of the fatty acid substrate with concomitant reduction of the ferric−hydroxide center to a ferrous−water species and formation of a fatty acid radical. Substrates with a weak C−H bond reduce **2** to generate a radical species and **1**. The reactivity profile with a variety of substrates is consistent with a HA mechanism and provides chemical precedent for the C−H bond activation step in the proposed mechanism of LO. The ability to predict substrate C−H bond dissociation energies, such as that of linoleic acid, with the bond strength approach is a useful tool in the understanding of metal-mediated HA in metalloenzymes.

This model reactivity supports the currently proposed mechanism of LO and provides a thermodynamic justification for HA by simple ferric−hydroxide species. Comparisons to other hydrogen abstracting species suggest that sterics and/or structural reorganization complicate the relation between ΔH° and the rate of HA as compared to organic radicals.

Experimental Section

Syntheses. All starting materials were purchased from Aldrich and used without further purification unless noted otherwise. $Fe^{II}(OTf)_2$ was synthesized according to a literature method.[96] Sodium hydride (60% oil dispersion) was washed with hexanes and dried in a vacuum. All solvents and gases were of analytical grade and were purified by literature methods.[97] CH_2Cl_2 and MeCN were distilled from CaH_2 under N_2 and stored over 4 Å molecular sieves. MeOH was distilled from $Mg(OMe)_2$ under N_2 and stored in darkness over 4 Å molecular sieves. Anhydrous diethyl ether (ether) was stored over 4 Å molecular sieves. THF was distilled from Na under N_2. 1,4-Cyclohexadiene and ethyl linoleate were dried over CaH and vacuum transferred under N_2. 9,10-Dihydroanthracene was sublimed and recrystallized from EtOH. Fluorene and xanthene were recrystallized twice from EtOH. 2,3-Dimethyl-2-butene, 4-methyl-1,3-pentadiene, and tetrahydronaphthalene were dried over $CaSO_4$ and distilled under N_2. Toluene, toluene-d_8, and ethylbenzene were washed with cold concentrated H_2SO_4, water,

(95) Novak, M. J.; Clapp, C. H.; Senchak, S. E.; Stover, T. J.; Potter, T. C.; Findeis, P. M. *J. Am. Chem. Soc.* **2001**, *123*, 747−748.

(96) Haynes, J. S.; Sams, J. R.; Thompson, R. C. *Can. J. Chem.* **1981**, *59*, 669−678.

(97) Perrin, D. D.; Armarego, W. L. F. *Purification of Laboratory Chemicals*, 1st ed.; Pergamon Press: New York, 1988.

10% $NaHCO_3$, and again water until the washings were neutral. After drying with $MgSO_4$, these substrates were distilled from Na. All iron complexes for crystallographic analysis were synthesized and handled under a N_2 inert atmosphere using a MBraun Labmaster 130 glovebox or standard Schlenk-line techniques. Flash column chromatography was performed using Silica Gel 60, 230−400 mesh from EM Science (Gibbstown, NJ) using standard techniques.[98]

Instrumentation. ^{1}H NMR spectra were recorded on a Varian Gemini-400 (400 MHz) NMR spectrometer at RT, and chemical shifts are reported in ppm downfield from an internal TMS reference. Electronic spectra at RT were measured on a Polytec X-dap fiber-optics UV/vis diode array spectrophotometer. Electronic paramagnetic resonance (EPR) spectra were recorded on a Bruker ER 220D-SRC instrument as frozen solutions at 77 K at X-band frequency in quartz tubes. EPR spectra were fit using Bruker Simfonia 1.25. Electrochemical measurements were recorded at 100 mV/s under N_2 at RT using a Bioanalytical Systems, Inc. CV-50W voltammetric analyzer, a platinum working electrode, a platinum wire auxiliary electrode, 0.1 M (n-Bu_4N)(ClO_4) supporting electrolyte, and a silver/silver chloride wire reference electrode, with all potentials referenced to the ferrocenium/ferrocene couple (in MeOH = +0.610 V vs SHE, ΔE = 0.080 V).[56] Solution magnetic moments were determined in MeOH-d_4, acetone-d_6, and $CDCl_3$ at RT by the Evans method.[47] Solid-state magnetic susceptibility measurements were performed with a SQUID magnetometer on a Magnetic Property Measurement System model 1822 at 298 K. Gas chromatography−mass spectroscopy (GC−MS) data were collected on a Hewlett-Packard 5890 system. Mass spectroscopy data (positive FAB and LSIMS) were collected by the Mass Spectrometry Facility, Department of Pharmaceutical Chemistry, University of California, San Francisco. Elemental analyses were performed by Midwest Microlabs (Indianapolis, IN).

Ligand Syntheses. 2,6-Bis(bis(2-pyridyl)carbinol)pyridine (PY5-OH). A dioxane solution containing 2,6-pyridinedicarboxylic acid (5.16 g) and excess thionyl chloride was heated at reflux for 4 h, and the solvent was removed to give a quantitative yield of 2,6-pyridinedicarbonyl chloride.[99] A THF solution (500 mL) of 2-bromopyridine (19.75 g) was cooled to −78 °C, and n-BuLi (50 mL, 2.5 M in hexane) was added dropwise to maintain the temperature below −60 °C. Slow addition of a THF solution (50 mL) of the acid chloride (6.26 g) at −78 °C to this lithopyridine solution was followed by quenching with MeOH (50 mL) and warming the solution to RT. After the addition of water (50 mL) and 10% HCl (100 mL), the organic components were removed, and the aqueous solution was washed with CH_2Cl_2. NaOH was added to the solution until basic, and the product was extracted with CH_2Cl_2. Evaporation of the CH_2Cl_2 solution gave a crude product that did not readily crystallize. The product was purified by flash column chromatography (5% MeOH/CH_2Cl_2) followed by crystallization from acetone/ether (7.05 g, 50%). ^{1}H NMR (400 MHz, $CDCl_3$): δ (ppm) 7.15 (4 H, t of d, J_1 = 3.0 Hz, J_2 = 1.0 Hz, 5-Hpy-a), 7.18 (2 H, d, J = 1.6 Hz, 3-Hpy-b), 7.42 (4 H, d, J = 5.2 Hz, 3-Hpy-a), 7.50 (1 H, t, 4-Hpy-b), 7.52 (4 H, t of d, J_1 = 5.2 Hz, J_2 = 1.0 Hz, 4-Hpy-a), 7.74 (2 H, s, C−OH), 8.49 (4 H, d, J = 3.0 Hz, 6-Hpy-a). ^{13}C NMR (400 MHz, $CDCl_3$): δ (ppm) 120.6, 122.3, 123.3, 136.2, 137.5, 147.5, 162.6. Mass spectroscopy (FAB^+, MH^+): m/e 448.1 (EM = 447.2).

2,6-Bis(bis(2-pyridyl)methoxymethane)pyridine (PY5). Dimethylation of **PY5-OH** (6.18 g) was performed in DMF (100 mL) using 2 equiv of NaH (0.70 g) and 2 equiv of iodomethane (4.12 g) at RT for 1 h. The solution was acidified with 10% HCl (30 mL) to dissolve the product in the aqueous layer, and the DMF was removed by extraction with CH_2Cl_2. NaOH was added to the aqueous solution until basic, and the product was extracted with CH_2Cl_2. The crude product collected from evaporation of the CH_2Cl_2 solution was purified by crystallization from cold acetone/ether (5.65 g, 85%). Colorless X-ray quality crystals were grown from an acetone/ether solution. ^{1}H NMR (400 MHz, $CDCl_3$): δ (ppm) 3.07 (6 H, s, C−OMe), 7.10 (4 H, t of d, J_1 = 3.0 Hz, J_2 = 1.2 Hz, 5-Hpy-a), 7.34 (4 H, d, J = 5.0 Hz, 3-Hpy-a), 7.42 (2 H, d, J = 5.6 Hz, 3-Hpy-b), 7.52 (4 H, t, J = 5.0 Hz, 4-Hpy-a), 7.64 (1 H, t, J = 5.6 Hz, 4-Hpy-b), 8.33 (4 H, d, J = 3.0 Hz, 6-Hpy-a). ^{13}C NMR (400 MHz, $CDCl_3$): δ (ppm) 53.2, 121.4, 121.7, 121.8, 125.0, 135.5, 136.9, 148.2. Mass spectroscopy (FAB^+, MH^+): m/e 476.1 (EM = 475.2).

Metal Complex Syntheses. [Fe(PY5)(MeOH)](OTf)$_2$ (1). Equimolar amounts of **PY5** (0.51 g) and $Fe(OTf)_2$ (0.38 g) were dissolved in MeOH (25 mL) under N_2. Addition of ether resulted in the precipitation of a yellow compound in nearly quantitative yield (0.85 g, 92%). Yellow-green crystals suitable for X-ray analysis were obtained from a MeOH/ether solution of the complex, [Fe(**PY5**)(MeOH)](OTf)$_2$·(MeOH). Absorption spectrum (MeOH): λ_{max} (nm), ϵ (M^{-1} cm^{-1}) 370, 1650; 785, 14; 865, 11. Cyclic voltammetry (MeOH): +0.930 V vs SHE (ΔE = 0.140 V). Solution magnetic moment (acetone-d_6, 292 K): μ_{eff} = 4.7 μ_B. ^{1}H NMR (400 MHz, acetone-d_6): δ (ppm) −11.3, 13.7, 15.8, 42.4, 53.5, 57.0. Elemental analysis: calcd for $C_{32}H_{33}N_5O_{11}F_6S_2Fe$ C, 42.83; H, 3.70; N, 7.80; found C, 42.46; H, 3.38; N, 7.76.

[Fe(PY5)(OMe)](OTf)$_2$ (2). Addition of 0.5 equiv of iodosobenzene (0.044 g) to a solution of [Fe^{II}(**PY5**)(MeOH)](OTf)$_2$ (0.32 g) in MeOH (20 mL) gave a red-orange ferric species at RT. The solution was removed and the orange crystalline material washed with ether. Recrystallization from a MeOH/ether solution of the complex resulted in red-orange crystals suitable for X-ray analysis (0.24 g, 75%), [Fe^{III}(**PY5**)(OMe)](OTf)$_2$·MeOH. Absorption spectrum (MeOH): λ_{max} (nm), ϵ (M^{-1} cm^{-1}) 337, 3600. Electron paramagnetic resonance (MeOH): (T = 77 K) g = 2.25, 2.16, and 1.96. Cyclic voltammetry (MeOH): irreversible reduction potential = +0.710 V vs SHE (Fc^+/Fc in MeOH = +0.610 V vs SHE). Solution magnetic moment (CD_3OD, 292 K): μ_{eff} = 5.3 μ_B. ^{1}H NMR (400 MHz, $CDCl_3$): δ (ppm) −7.1, 12.5, 15.7, 45.3, 55.6, 60.2. Elemental analysis: calcd for $C_{32}H_{30}N_5O_{10}F_6S_2Fe$ C, 43.76; H, 3.44; N, 7.97; found C, 43.57; H, 3.28; N, 7.76.

[Fe(PY5)(CH_3CN)](OTf)$_2$ (3). Equimolar amounts of **PY5** (0.11 g) and $Fe(OTf)_2$ (0.09 g) were dissolved in CH_3CN (5 mL) under N_2 to give a deep orange-brown solution. A brown crystalline solid was isolated after addition of ether (0.15 g, 75%). If dried under vacuum or kept in an unsealed container, loss of the coordinated CH_3CN results in a pale yellow compound. Orange-brown crystals grown in an CH_3CN/ether solution are stable in ether solution. Absorption spectrum (CH_3CN): λ_{max} (nm), ϵ (M^{-1} cm^{-1}), 362, 6900; 384, 6900; 424, 5880; 554, 175. Cyclic voltammetry (CH_3CN): +1.150 V vs SHE (ΔE = 0.090 V). Solution magnetic moment (CD_3CN, 292 K): μ_{eff} = 0 μ_B. ^{1}H NMR (400 MHz, CD_3CN): δ (ppm) 4.08 (6 H, s, C−OMe), 7.74 (4 H, d of d, J = 4.1 Hz, 3-Hpy-a), 8.01 (4 H, t, J = 7.6 Hz, 4-Hpy-a), 8.20 (1 H, t, J = 9.2 Hz, 4-Hpy-b), 8.30 (4 H, d, J = 7.3 Hz, 5-Hpy-a), 8.37 (2 H, d, J = 8.6 Hz, 3-Hpy-b), 9.97 (4 H, d, J = 4.6 Hz, 6-Hpy-a). The perchlorate analogue of this compound has been previously reported.[36]

[Fe(PY5)(OMe)](OTf) (4). Addition of triethylamine (0.3 mL, 18 equiv) to a solution of [Fe(**PY5**)(MeOH)](OTf)$_2$ (0.11 g) in MeOH (10 mL) under N_2 resulted in a cloudy red-orange solution at RT. After filtration of the solution, addition of ether resulted in the precipitation of an orange compound (0.024 g, 25%). Absorption spectrum (MeOH): λ_{max} (nm), ϵ (M^{-1} cm^{-1}), 340, 1300; 440, 1700; 715, 30. Cyclic voltammetry (MeOH): +0.760 V vs SHE (ΔE = 0.100 V). Solution magnetic moment (acetone-d_6, 292 K): μ_{eff} = 4.6 μ_B. ^{1}H NMR (400 MHz, acetone-d_6): δ (ppm) −10.8, 14.1, 15.8, 39.0, 54.3, 60.1.

Substrate Syntheses. 2,4,6-Tri-*tert*-butylphenol-*d* (TTBP-*d*). 2,4,6-Tri-*tert*-butylphenol (0.13 g) was dissolved in DMSO-d_6 (3.0 mL) along with 0.010 g of NaH under N_2. The solution was stirred overnight and then quenched with 5.0 mL of D_2O. White precipitate was collected, washed with D_2O, and dried under vacuum (0.12 g, 90%). GC−MS indicated deuteration of >99%. ^{1}H NMR (400 MHz, $CDCl_3$): δ (ppm) 7.20 (2H, s), 1.45 (18 H, s), 1.30 (9 H, s).

(98) Still, W. C.; Kahn, M.; Mitra, A. *J. Org. Chem.* **1978**, *43*, 2923−2925.
(99) Bessard, Y.; Crettaz, R. *Heterocycles* **1999**, *51*, 2589−2602.

9,10-Dihydroanthracene-d_4 (DHAn-d_4). 9,10-Dihydroanthracene (3.02 g) was dissolved in DMSO-d_6 (8.0 mL) along with 0.19 g of NaH under N_2. After the deep red solution was stirred at RT for 2 h, the reaction was quenched with D_2O (5 mL), and the crude product was filtered and washed with copious amounts of H_2O. ^{1}H NMR ($CDCl_3$) indicated deuteration of ~90%. The above reaction was repeated, and the deuterated product was recrystallized twice from EtOH (2.78 g, 90%). GC−MS indicated deuteration of >99%. ^{1}H NMR (400 MHz, $CDCl_3$): δ (ppm) 7.18 (4H, m, 1-H), 7.33 (4H, m, 2-H), no resonance peak at 3.95, as in DHAn.

1,4-Cyclohexadiene-d_8 (CHD-d_8). A modified Birch reduction of benzene was used.[100] To anhydrous liquid NH_3 (75 mL), cooled to 233 K, was added benzene-d_6 (3.25 g), ethanol-d_6 (5.46 g), and diethyl ether (8.45 g). Sodium metal (2.61 g) was added slowly over 2 h, so as to maintain the temperature of the reaction below the boiling point of NH_3 (−33 °C). The reaction was quenched with Decalin (15 mL) and ice water (40 mL). The organic layer was washed with copious amounts of water followed by 1 M HCl. After drying with $MgSO_4$, the product was distilled from Decalin under N_2, discarding the first fraction of ethanol. A second distillation under N_2 gave CHD-d_8 in good purity (2.44 g, yield = 75%). GC−MS indicated deuteration of >99%. ^{1}H NMR (400 MHz, $CDCl_3$): δ (ppm) no resonance peaks.

X-ray Crystallography. ORTEP representations with a detailed numbering scheme and complete tables of positional parameters, bond lengths, bond angles, and anisotropic thermal factors for the crystal structures described below are provided in the Supporting Information.

For each of the X-ray crystal structures presented, the data set was collected at a temperature of 203 K using the ω scan technique. A suitably sized crystal was mounted in paratone oil on a glass fiber and placed in a cold stream of N_2 on an Enraf-Nonius CAD-4 diffractometer with graphite-monochromated Mo Kα radiation ($\lambda = 0.71073$ Å). Unit cell parameters and an orientation matrix for data collection were typically obtained from a least-squares refinement using the setting angles of 25 carefully centered reflections in the range $19.00° < 2\theta < 36.00°$. Structural and refinement data for **PY5**, **1**, and **2** are summarized in Table 2. Moving-crystal moving-counter background measurements were made by scanning an additional 25% above and below the scan range. The counter aperture consisted of a variable horizontal slit with a width ranging from 2.0 to 2.5 mm and a vertical slit set to 2.0 mm. Three intensity-check reflections were monitored hourly to determine if there was any significant crystal decay due to X-ray exposure. Unless noted below, a correction factor was not applied. An empirical absorption correction based on azimuthal scans of several appropriate reflections was applied to all of the data sets. The data were corrected for Lorentz and polarization effects. The structures were solved by direct methods and expanded using Fourier techniques. All non-hydrogen atoms were refined anisotropically, unless noted below. Hydrogen atoms were located by difference Fourier maps but included at an idealized position 0.95 Å from their parent atoms for the final refinement. Isotropic thermal parameters 1.2 times the parent atoms were assumed. Unless otherwise noted, the remaining significant peaks on the final difference Fourier maps of **1** and **2** were located near the triflate anion(s). Neutral atom scattering factors were taken from Cromer and Waber.[101] Anomalous dispersion effects were included in F_{calc},[102] the values for $\Delta f'$ and $\Delta f''$ were those of Creagh and McAuley.[103] The values for the mass attenuation coefficients are those of Creagh and Hubbell.[104] All calculations were performed using the teXsan crystallographic software package from Molecular Structure Corporation. Specific details for each of the crystal structures are found in the Supporting Information.

pK_a Measurements. The pK_a of [Fe^{II}(**PY5**)(MeOH)]$^{2+}$ was determined by spectrophotometric titrations with two bases: 2,6-lutidine (pK_a(MeOH) of cation = 6.8)[105] and *N*-methylmorpholine (pK_a(MeOH) of cation = 8.4 as measured against bromocresol green, pK_a(MeOH) = 9.8[106]). Each scan was fit to the best linear combination of pure **1** and **4** through a least-squares fit criterion in an Excel spreadsheet. From the relative concentrations of **1** and **4** and the known stoichiometry of the base added, a pK_a can be obtained.

Kinetic Measurements. Kinetic experiments were performed in rigorously dried solvents. MeOH (Aldrich, 99.8+%) was refluxed over Mg turnings and iodine until the iodine color disappeared. The dried solvent was distilled from $Mg(OMe)_2$ under N_2 and stored in darkness in the drybox over molecular sieves, 4 Å. CH_3CN (99.8%) was refluxed over CaH and then distilled under N_2. The dried solvent was stored in darkness in the drybox over molecular sieves, 4 Å.

The kinetic data were measured with a Polytec X-dap fiber-optics UV/vis diode array spectrophotometer. The reaction cell was maintained at a constant temperature using an FTS Systems model MC480A1 multitemperature bath. MeOH and MeCN solutions of **2** were prepared in the drybox or on a N_2 line using standard Schlenk techniques directly before use. Substrate was added directly to the solvent, and the solution was transferred to the reaction vessel. A fiber-optic dip-probe was inserted into the solution (path length = 0.1 or 1.0 cm), and the vessel was carefully sealed. For kinetic experiments in the presence of O_2, the initial N_2 was removed by continuous purging of the reaction vessel with O_2. Data collection was delayed for 5 min to allow for complete diffusion of O_2 into the reaction mixture.

All kinetic runs were performed with an excess of substrate to achieve pseudo-first-order conditions for the reduction of the ferric complex. The reduction of [Fe^{III}(**PY5**)(OMe)]$^{2+}$ was measured over the wavelength range from 300 to 450 nm, which includes the band maxima for all three relevant ferric and ferrous complexes. A constant concentration of **2** (2.25×10^{-3} M) was used in all reactions, while the substrate concentration ranged from 0.20 to 2.00 M and was adjusted to achieve a reasonable rate of ferric complex reduction. For the reactions run in MeOH, the reduction of **2** to **1** was monitored, and in MeCN, the reduction of **2** to **3** was monitored. The reactions were run to near completion (greater than 5 half-lives of **2**) in all kinetic measurements except for that of toluene. These reactions were exceptionally slow and were only run to greater than 2 half-lives of **2**. All reactions remained homogeneous throughout the data collection.

Spectral deconvolution and kinetic analyses were determined using the Specfit software package. The data were corrected to remove substrate or product peaks in the iron region of the spectra when these features interfered with the kinetic analyses. The rate constants were determined from absorption data collected in the wavelength range 300−450 nm. For each substrate, at least four measurements were made of k_{obs} with differing substrate concentrations in the range of 0.20−2.0

(100) Brandsma, L.; van Sodingen, J.; Andringa, H. *Synth. Commun.* **1990**, *20*, 2165−2168.
(101) Cromer, D. T.; Waber, J. T. *International Tables for X-ray Crystallography*; Kynoch: Birmingham, 1974; Vol. IV.
(102) Ibers, J. A.; Hamilton, W. C. *Acta Crystallogr.* **1964**, *17*, 781−782.
(103) Creagh, D. C.; McAuley, W. J. In *International Tables for Crystallography*; Wilson, A. J. C., Ed.; Kluwer Academic Publishers: Boston, 1992; Vol. C, pp 219−222, Table 4.2.6.8.
(104) Creagh, D. C.; Hubbell, J. H. In *International Tables for Crystallography*; Wilson, A. J. C., Ed.; Kluwer Academic Publishers: Boston, 1992; Vol. C, pp 200−206, Table 4.2.4.3.
(105) Covington, A. K.; Dickinson, T. *Physical Chemistry of Organic Solvent Systems*; Plenum Press: London, 1973; p 823.
(106) Dean, J. A. *Lange's Handbook of Chemistry*, 15th ed.; McGraw-Hill: New York, 1999; Vol. 1.
(107) Bordwell, F. G.; Cheng, J.-P.; Ji, G.-Z.; Satish, A. V.; Zhang, X. *J. Am. Chem. Soc.* **1991**, *113*, 9790−9795.
(108) Berkowitz, J.; Ellison, G. B.; Gutman, D. *J. Phys. Chem.* **1994**, *98*, 2744−2765.
(109) Arends, I. W. C. E.; Mulder, P.; Clark, K. B.; Wayner, D. D. M. *J. Phys. Chem.* **1995**, *99*, 8182−8189.
(110) Luo, Y.-R.; Holmes, J. L. *J. Phys. Chem.* **1994**, *98*, 303−312.
(111) Rodgers, A. S.; Wu, M. C. R. *J. Am. Chem. Soc.* **1973**, *95*, 6913−6917.
(112) Stein, S. E.; Brown, R. L. *J. Am. Chem. Soc.* **1991**, *113*, 787−793.
(113) Rossi, M. J.; McMillen, D. F.; Golden, D. M. *J. Phys. Chem.* **1984**, *88*, 5031−5039.
(114) Pedley, J. B.; Naylor, R. D.; Kirby, S. P. *Thermochemical Data of Organic Compounds*; Chapman and Hall: London, 1986.
(115) Lind, J.; Shen, X.; Eriksen, T. E.; Merényi, G. *J. Am. Chem. Soc.* **1990**, *112*, 479−482.

M. The absolute second-order rate constants k_2 were calculated by a least-squares fitting plot of k_{obs} versus substrate concentration.

Kinetic experiments were analyzed for products following each run. The reaction mixture was concentrated to near dryness, dissolved in ether, and washed with 0.1 M NaOH followed by 1 M HCl solutions to remove the iron and ligand. Following this workup, the following products were identified by GC−MS (starting substrate in parentheses): anthracene (DHAn), benzene (CHD), 1,2-dihydronaphthalene (tetralin), and α-methylstyrene (cumene). The other organic products either were generated in quantities below the level of detection or were removed in the base/acid workup. When a proposed radical intermediate could lose an additional hydrogen to form an olefin, the resultant olefin was proposed to be the product, based on the aforementioned products for similar reactions. Because of the large excess of substrate needed to run the reactions on a convenient time scale, accurate yields could not be measured for most kinetic experiments.

Acknowledgment. We thank Dr. Uma Sundaram for useful discussions. We are grateful to the National Institutes of Health (GM50730) and the Stanford Graduate Fellowship Fund (C.R.G.) for financial support of this work.

Supporting Information Available: Experimental data for variable-temperature solution magnetic susceptibility measurements for **1** and **2**; kinetic data for Table 3; plot of k_{2corr} versus substrate pK_a; Eyring plot of the DHAn reduction of **2** over 298−343 K; structure reports for **PY5**, **1**, and **2** (PDF). This material is available free of charge via the Internet at http://pubs.acs.org.

JA016451G